UNIVERSIDAD AUTÓNOMA DE MADRID
ESCUELA POLITÉCNICA SUPERIOR
DEPARTAMENTO DE TECNOLOGÍA Y DE LAS COMUNICACIONES

FEATURE EXTRACTION FOR BIOMETRIC RECOGNITION USING MILLIMETRE-WAVE IMAGES

–TRABAJO FIN DE MÁSTER–

EXTRACCIÓN DE CARACTERÍSTICAS PARA EL RECONOCIMIENTO BIOMÉTRICO A TRAVÉS DE ONDAS MILIMÉTRICAS

Author: Ester González Sosa
Ingeniero de Telecomunicación,
Universidad de Las Palmas de Gran Canaria

A Thesis submitted for the degree of:

Máster Oficial Universitario en Investigación e Innovación en TIC
(Master of Science)

Madrid, October 2013

Colophon

This book was typeset by the author using LaTeX2e. The main body of the text was set using a 11-points Computer Modern Roman font. All graphics and images were included formatted as Encapsuled Postscript (^{TM} Adobe Systems Incorporated). The final postscript output was converted to Portable Document Format (PDF) and printed.

Departmento:	Tecnología Electrónica y de las Comunicaciones Escuela Poliétcnica Superior Universidad Autónoma de Madrid (UAM), SPAIN
Título:	Feature Extraction for Biometric Recognition using Millimetre-Wave Images
Autor:	**Ester González Sosa** Ingeniero de Telecomunicación (Universidad de Las Palmas de Gran Canaria)
Director:	**Dr. Rubén Vera Rodríguez** Doctor Ingeniero de Telecomunicación (Swansea University, UK) Universidad Autónoma de Madrid, SPAIN
Tutor:	**Prof. Julián Fiérrez Aguilar** Doctor Ingeniero de Telecomunicación (Universidad Politécnica de Madrid) Universidad Autónoma de Madrid, SPAIN
Fecha:	10 de Octubre de 2013
Tribunal:	**Prof. Javier Ortega García** Universidad Autónoma de Madrid, SPAIN **Dr. Julián Fiérrez Aguilar** Universidad Autónoma de Madrid, SPAIN **Prof. José María Martínez Sánchez** Universidad Autónoma de Madrid, SPAIN
Suplente:	**Prof. Daniel Ramos Castro** Universidad Autónoma de Madrid, SPAIN
Calificación:	

The research described in this Thesis was carried out within the Biometric Recognition Group – ATVS at the Dept. of Tecnología Electrónica y de las Comunicaciónes, Escuela Politécnica Superior, Universidad Autónoma de Madrid. The project was funded by the Obra Social La Caixa-Convocatoria 2012.

Abstract

The use of Millimetre-Wave images (MMW) has been proposed recently in the biometric field aiming to overcome certain limitations when using images acquired at visible frequencies.

In this work, a body-shape based biometric system has been developed using the information of the human contour extracted from MMW images. Images are extracted from the BIOGIGA, a synthetic database which simulates the effect of the 94 GHz radiation over the human body. The images of this database are obtained from real measures from 50 people.

We propose several methods for the parameterization and classification stage with the objective of finding the best configuration of the biometric-system. Among the methods proposed for the parameterization stage we find: the contour coordinates, which constitutes the baseline technique; shape contexts descriptor which uses a log-polar histogram to describe the relative situation of all the points within the shape with respect to an specific point; Fourier Descriptors, that applies the Fourier transform to the contour coordinates; and finally landmarks, a reduced set of points which describes some singular points within the human-body shape. In the classification stage, we use two methods: a naive classifier, the Euclidean distance (ED) and a classifier based on dynamic programming, dynamic time warping algorithm (DTW).

Several experiments are carried out with the objective of selecting the most discriminative feature set and classifier from all the proposed approaches. The experiments are developed following two main types of protocols, depending on the number of images use per person in the training and evaluation stage.

The results show to what extent the DTW improves the performance of the system with the respect to the baseline Euclidean distance and the necessity of a high resolution of the contour in order to obtain a good performance of the system. The use of the contour coordinates is the most suitable feature to use in the system regarding the performance and the computational cost involved. Even though the results obtained with more complex features such as shape contexts or Fourier descriptors are quite reasonable, their computational cost makes them less appropriate for practical scenarios.

The results obtained in this work are compared with other previous works which are based on geometrical distance measures between some landmarks within the shape of the body. Apart from improving some of these results obtained in this previous work, we consider that the system developed in this Masther Thesis based on applying Contour Coordinates with DTW is much more robust and suitable for real MMW images compared the distance-based system, whose capability of accurately extracting the body landmarks would drop in realistic scenarios.

A mi querida familia

No existe gran talento sin gran voluntad.
H. Balzac

Acknowledgements

This MSc Thesis summarizes the work carried out during my Master studies with the Biometric Recognition Group - ATVS during the course 2012/2013.

First of all, I would like to thank my advisors Dr. Ruben Vera and Prof. Julian Fierrez for the supportive help and their guidance throughout all this year. Thanks Ruben for the daily support, and the time invested in all my educational duties.

I would also like to express gratitude for Prof. Javier Ortega for giving me the opportunity to work with this group during this entire course.

Of course, I have to thank all my colleagues from the ATVS group: my academicals coetaneous: Alicia Lozano, Alvaro Dieguez, Fernando Espinoza and the other colleagues from the lab: Pedro Tome (thanks for all the help during my beginning in ATVS), Marta Gomez, Javier Franco, Ruifang Wang, Daniel Ramos and Javier Gonzalez. I would like to mention Javier Eslava, Sara Garcia, Fatima Garcia and Sandra Uceda for all the good times we have passed working hard. I do not want to forget my classmates: Rafa, Luis, Rut, Yvonne, Marta, Pablo, Raul, Derlin, Augusto, Cesar and Julio.

Last but not least I would like to thank all my family: my parents Daniel y Rita which has been always on my side unconditionally; my beloved brothers: Isabel (thanks for being always there), Santiago, Roberto and Gabriel; my grandparents Maria Dolores, Santiago, Tere, Luisa and all my aunts, uncles, and cousins (specially Cristina, Elias y Pablo) for being always there to celebrate my success and sweeten the less joyful moments. There are some people that we should call family as well, but we referred to them as friends. I am very fortunate to have all of them, my lifelong friends, my dear flatmates and all the rest of friends with whom I share part of my life.

Gracias.

Ester González Sosa
Madrid, October 2013

Contents

List of Figures

List of Tables

Chapter 1

Introduction

Traditionally, biometric systems have been working in the visible band due to the simplicity of the acquisition systems. However, this region of the spectrum suffers from several limitations caused mainly by the light conditions, shadows, and occlusions in the body. Aiming to solve all this drawbacks, some researchers have proposed to acquire images in other regions of the spectrum such as X-rays [Chen and Jain, 2005; Shamir *et al.*, 2009], the infrared region [Li *et al.*, 2007], millimeter waves (MMW, 30-300 GHz) and submillimeter waves (SMW 300-3000 GHz) [Alefs *et al.*, 2010].

In this Dissertation, a work based on person identification through MMW images is carried out. To this aim, a 1200-images database corresponding to 50 people acquired at 94 GHz has been used. Although several works based on this database have built a biometric system using geometric distances between some key points of the human silhouette [Moreno-Moreno *et al.*, 2011b], in this work a contour-based biometric system has been developed using different shape matching techniques.

In this chapter biometrics are introduced in Section 1.1, and several aspects, closely related to the topic at hand, are described: in Section 1.2, multibiometrics are presented and Section sec:intro:applications describes the main applications in biometrics. Finally, the movitation and objectives of this work will be briefly explained in Section 1.4.

1.1. Biometric Systems

A biometric system measures one or more physical or behavioral characteristics of an individual to determine or verify his identity" [Jain *et al.*, 1999, 2011]. Biometric systems can be therefore regarded as a specific application of pattern recognition algorithms. Our society has always considered essential the privacy of the confidential information. Although the scientific history of biometrics was not developed until 30 years ago, some previous historical facts exist and show the continuous effort of the human being to find identification techniques.

In Occident, in 1883, the French Alphone Bertillon proposes the anthropometric method, composed of a set of length and width measures of the body and individual marks with the

(a) Dynamic biometric trait (b) Static biometric trait

Figure 1.1: *Examples of Dynamic biometric trait (left) and Static biometric trait (right)*

objective of identifying criminals [Gloor, 1980]. Nowadays, thanks to the development of computer science within the technological era, we can find in the market reliable solutions based on biometrics [Jain *et al.*, 1999]. The very first trait that emerges from biometrics is the fingerprint, conceived as the biometric trait par excellence. Gradually, new biometric traits are considered, providing a wide variety of options and a high security level as well.

Traditionally, a user could be identified through something known only for the user, such as a password, or something owned exclusively by him/her, for instance: a card. The main inconvenience of these methods relies on the high facility of misappropriation of the user's identity.

Biometrics appears in order to avoid all these threads. From now on, the subject is not recognized by what he/she knows nor what he/she has but by what he/she is. Specifically, biometrics take advantage of physical or behavior features for the identification process. A biometric trait may be defined as **static** when the information involved in the system deals with what the person is, and **dynamic** when information about what the person does is used to build the biometric system [Jain *et al.*, 2004]. Fig.1.1 shows an example of these two types of biometric traits. The static biometrics is based mainly on physical traits while dynamic biometrics is based on behaviour traits. Another typical classification of biometric traits consist of dividing them into physical and behavior traits. The main physical traits are fingerprint, face, iris, retina, hand geometry, palm print, knuckles, vein pattern, DNA, ear. Among the most important behavioral traits, we find signature, voice, gait, corporal movements, etc. Fig.1.2 show some examples of different biometric traits.

In order to consider a biometric trait feasible, this has to possess some properties, among them:

- **Universality**: Every person needs to have this biometric trait.
- **Distinctiveness**: The trait has to be unique of every single person, or at least discriminating enough to distinguish between two subjects.

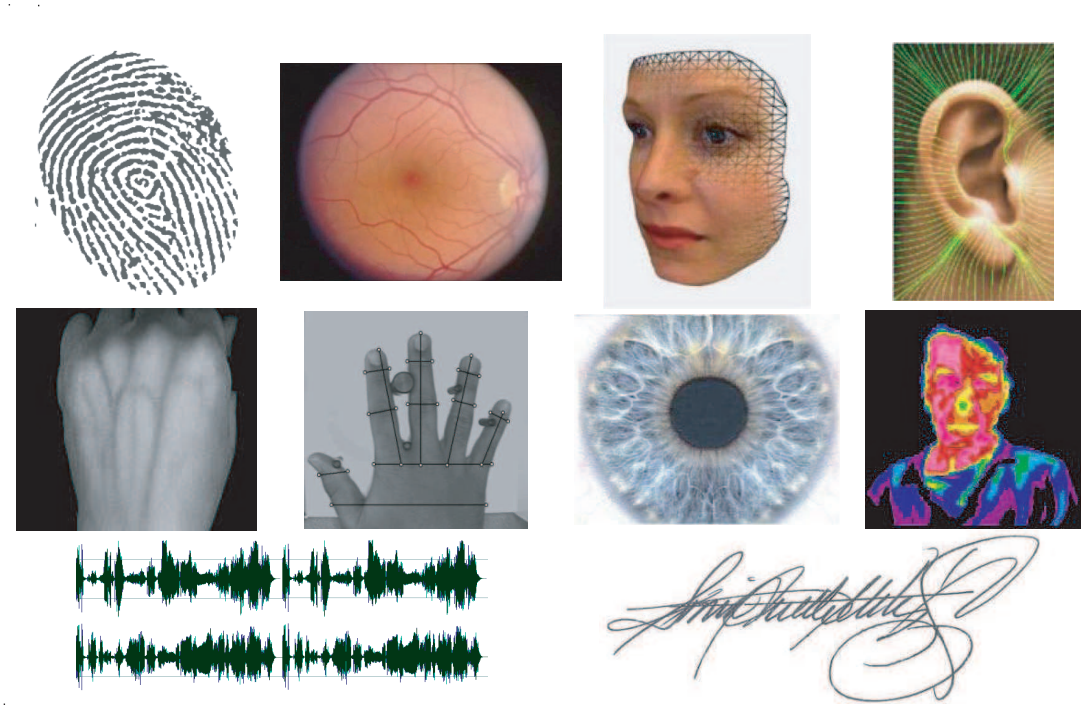

Figure 1.2: *Examples of common biometrics.*

- **Permanence**: must be a trait permanent along time, as steady as possible.
- **Collectability**: this biometric trait has to be easily measured quantitatively.

Apart from these aforementioned characteristics that any biometric trait should have, the biometric system in which the trait is involved requires to take into account these practical criteria:

- **Quality-cost relation**: the requirements of any biometric system depend on the type of scenario which is required for.
- **Acceptability**: the perception the user has to the system need to be taken into account .
- **Robutness**: a biometric system should be robust enough to deal with fraud and risk of vulnerability.

A biometric system may be performed in two different modes: **identification** and **verification**. When a system works in the identification mode, the biometric system must answer the question: "Who is this person?" On the other hand, when the system works in the verification mode, the system must answer the question "Is this person who claims to be?"

The computation cost of each mode is different. In the **identification** mode, a **one-to-many** comparison must be performed in order to compare the model of the input identity

versus the remainder models within the database. As a result, the system returns an identity when the subject is in the database or a negative response, otherwise.

On the contrary, in the **verification** mode, a **one-to-one** comparison is accomplished, contrasting the model of the input identity versus the model of the claimed identity. In this mode, the system gives back a yes/no response [Jain *et al.*, 2004]

1.2. Multibiometrics

The high quality requirements that society demands cannot be guaranteed by a single biometric trait. Besides, there is no biometric trait that satisfies all the aforementioned characteristics: while some biometric traits have a very high discrimination capability, they are relatively easy to circumvent. Until now, we have not found a biometric trait which is the best option for any kind of environment. The scientific community has proposed multibiometrics or the combination of several biometric traits as a promising solution to all these drawbacks: several sources usually compensate for the inherent limitations of one another [Ross *et al.*, 2006].

Multibiometrics can be accomplished in different ways according to the item that is fused:

- **Multimodality**: refers to the technique which comprises more than one biometric trait to build the biometric system. For instance: merging information from hand geometry and palmprint.
- **Multiinstance**: uses several samples of the same biometric trait as it may be the left iris and the right iris.
- **Multialgorithm**: more than one algorithm is applied to the same sample of biometric trait. For example: the usage of minutia-based algorithm and globally-based algorithm for palm print
- **Multisensor**: different sensors are used to acquire the biometric trait. The usage of a visible camera and an infrared camera is an example of a multisensor scheme.

The information offered by several unimodal biometric systems can be fused at five different levels, namely: *i*) sensor-level, *ii*) feature-level, *iii*) score-level, *iv*) rank-level, and *v*) decision-level. While the first two options fuse the information prior to matching, the remainder approaches use the information available after matching: either a numeric score or a binary decision (accept/reject). Even though fusion at an earlier processing stage should perform better, specific and more complex algorithms have to be applied. The development of such algorithms is not forthright, and therefore most multibiometric systems use score- or decision-level approaches.

Figure 1.3: *Chip of the Spanish National Identity Document.*

1.3. Main Applications of Biometric Systems

The applications of biometrics are countless. In all different types of scenarios where is used, biometrics aims to improve the security of the subject or some crucial information [Prabhakar *et al.*, 2003].

Its traditional use has been associated with forensic applications through DNA samples or fingerprint used to confirm the identity of the subjects.

Biometrics is applied to many different fields. For instance, in **airports**, the use of biometrics is emerging. The airport of *BenGurion*, Israel is considered one of the pioneers as has used a control security system based on biometrics since 1999 [Ben]. Among commercial security applications, biometrics can be found in ATM's, as well as in **telematic services** such as internet banking, database access, among others. biometrics also helps to improve the security of **access to commercial buildings**, as is the case of Walt Disney World Park Attraction, in which some hand biometric measures are taken in order to assure that a three-days pass is only used by the same person. The chip of the Spanish National Identity Document (see Fig.1.3) holds some biometric information on the subject related to his/her fingerprint, signature and face.

Biometrics may also be integrated in domotic systems, helping to access the dwelling, switching-off and switching-on of computers, car aperture, etc. More and more, biometric systems are being integrated within the design of smartphones, aiming to solve identification needs. The most common biometrics traits used in this case are speech, fingerprint, face and iris.

Other practical applications related to border control and natality control have emerged in the last few years. For instance, the US-VISIT program in the States aims to provide biometric identification services that help federal, state, and local government decision makers accurately identify people. The Unique Identification (UID) system in India, is collecting different biometric samples (iris, fingerprint and face) from all their citizens in order to solve the identification of very large numbers of subjects with negligible error rates [UID].

1.4. Motivation and Objectives

Many biometric characteristics are used to identify individuals: fingerprint, signature, iris, voice, face, hand, etc. The majority of these biometric traits are acquired with cameras working

at visible frequencies of the electromagnetic spectrum. Such images are affected by, among other factors, lighting conditions (shadows, reflections, etc.) and the body occlusion (e.g. clothing, make up, hair, etc.). To overcome these limitations, researchers have proposed the use of images acquired at other spectral ranges: X-ray (XR) [Chen and Jain, 2005], infrared (IR) [Li *et al.*, 2007], millimeter (MMW) [Alefs *et al.*, 2010] and submillimeter (SMW) waves [Appleby and Anderton, 2007; Moreno-Moreno *et al.*, 2009]. The images captured beyond the visible spectrum circumvent, to some extent, some of the mentioned limitations; furthermore, they are more robust to spoofing than other biometric images/traits.

Among the spectral bands out of the visible spectrum, the millimeter waves (with frequency in the band of 30-300 GHz) [Yujiri *et al.*, 2003] present interesting properties that can be exploited in biometrics: ability to pass through clothing and other occlusions, innocuous to health and the recent deployment and rapid progress of GHz-THz systems in screening applications.

Unlike imaging technology in the visible or infrared band, GHz-THz technology is under development [Mait *et al.*, 2009]. This fact, together with the privacy issues that the body images in this band present, have caused that, to date, there are no public databases with images of people acquired in that frequency range. In fact, there are just a few works on this field. Specifically, just one working with real data [Alefs *et al.*, 2010], and some others based on BIOGIGA database, which is a synthetic database [Moreno-Moreno *et al.*, 2011a]. Alefs *et al.* [2010] proposed a holistic recognition approach based on the texture information on the MMW images. On the other hand, the work by Moreno-Moreno *et al.* [2011b] proposes a biometric system based on geometric measures between different key points of the contour using MMW images from the BIOGIGA database. This shortage of biometric recognition research based on MMW images is due, in part, to the lack of databases of images of people acquired at GHz. This lack is a consequence of: *i*) the **privacy concerns** these images present, and *ii*) most of the imaging systems working at the MMW/SMW band are either in prototype form or **not easily accessible** for research.

In this work, we propose a novel approach for biometric recognition based on the comparison of body contours extracted from images at 94 GHz. This is inspired by previous works, which show that recognition through the shape and boundary of traits such as hand or signature are fairly reliable [Jain *et al.*, 2002; Yoruk *et al.*, 2006]. In fact, three approaches based on the body shape are considered: *i*) a baseline technique based on the Euclidean Distance, *ii*) a programming dynamic technique based on the dynamic time warping algorithm (DTW) and *iii*) a Shape Context descriptor. Several experiments are carried out to determine the performance and behavior of these different approaches. Also, different experimental protocols are followed varying the quantity of training data for different contour sizes. Finally, a comparison with the previous works based on geometric measures is also carried out.

The main objectives of this Dissertation are summarized in three points:

- Develope a **body-shape biometric system**: different appproaches to model the silhouette of people and considered. A navie classifier and a complex classifier are studied.

- Carry out a **comparison** among the chosen **shape matching techniques**: one of the main objectives of this work consists of finding the configuration that optimizes the performance of the system. This means that a combination of feature and classifier is proposed as the best configuration in order to improve the performance of the system.
- Comparison with the **distance-based biometric** system proposed by Moreno-Moreno *et al.* [2011b].

1.5. Outline of the Dissertation

The Dissertation is structured as follows:

- Chapter 1 introduces the topic of biometrics and gives the motivation, outline and objectives of this work.
- Chapter 2 summarizes the state of the art in biometrics beyond the visible range and shape matching, presenting related works.
- Chapter 3 describes the methods proposed in the work, either for features to model the shape of the contour and classifiers.
- Chapter 4 presents the experimental protocol followed in the experiments.
- Chapter 5 describes the experiments carried out and analyses the results.
- Chapter 6 concludes the Dissertation summarizing the main results obtained and outlining future research lines.

Chapter 2

Related Works and State of the Art

The goal of this work consists of developing a system able to identify people from their contours using images acquired in the MMW band.

Bearing this in mind, two main areas are presented in this chapter. First, as images from the database are acquired in the MMW band of the electromgnetic spectrum. The study of the state of the art of biometrics beyond the visible band has been based on the work made by Moreno Moreno [2012].

On the other hand, the novelty of this works relys on the possibility of identifying people from their contours. Hence, a brief review of the different shape matching techniques which has been used throughout the years is outlined.

2.1. Biometrics beyond the Visible Range

The ability to capture an image of the whole human body or a part of it has attracted much interest in many areas such as Medicine, Biology, Surveillance and Biometrics [Richards, 2001]. Images acquired at visible spectrum (VIS) are widely used; however they present some limitations, especially when they are used in these fields.

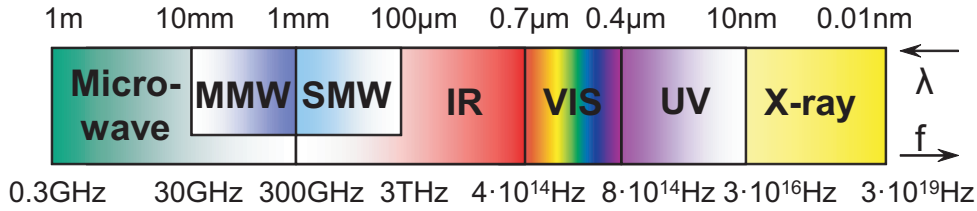

Figure 2.1: *Electromagnetic spectrum showing the different spectral bands between the Microwaves and the X-rays. IR band is sometimes considered to extend to 1 mm including the SMW region.*

As can be seen from Fig.2.1, there are other bands down the visible range and up the visible range that are used in different kind of body-based applications: IR, magnetic resonance, radioisotope, XR, acoustical, MMW-, SMW-imaging, biometric purposes. Only those bands

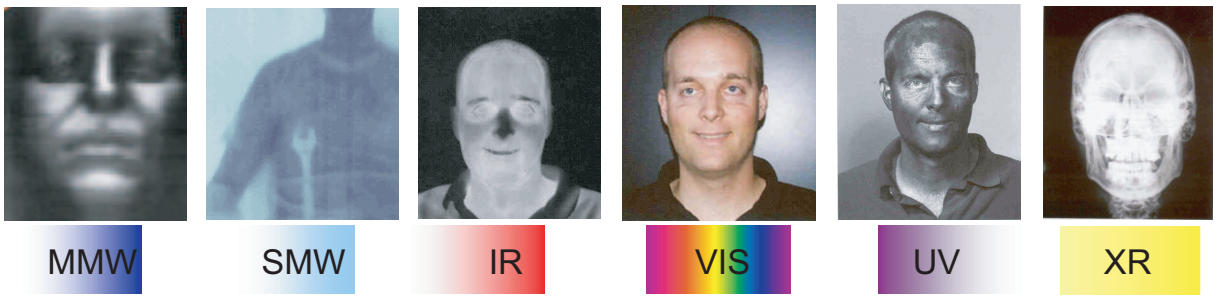

Figure 2.2: *Images acquired at different spectral bands.*

that do not have a high level of intrusiveness are suitable for biometric applications. Among them: IR, MMW and SMW imaging.

From Fig.2.2 it can be deduced also that the images acquired in different bands of the spectrum are very different between them. Depending on the band used, different properties of the subject such as appearance, temperature, skull, texture, etc. can be extracted. Those properties need to be considered when choosing a range of the spectrum for any imaging application.

The IR imaging technology is the most used in biometrics beyond the visible spectrum, followed by XR. On the other hand, the images acquired at the MMW/SMW band have been hardly used in biometrics. In fact the work by Alefs *et al.* [2010] and by Moreno-Moreno *et al.* [2011b] are, to date, the unique published research work about biometric recognition based on MMW/SMW images.

In this chapter, a brief review about IR and XR imaging technologies will be exposed. Then, the MMW/SMW imaging technology will be described in more detail.

2.1.1. Architectures

Imagery can be classified into two architectures: passive or active. In the former group the image is generated by **receiving** natural radiation which has been emitted and reflected from the scene, obtaining a map of brightness temperature. On the other hand, in active imaging the radiation is **transmitted** to the scene and then collected after reflection to form the image, which is a map of reflectivity.

The contrast in the scene in any part of the spectrum is a function of the optical properties of the object being imaged and its background. The main optical properties that are involved in this physical phenomenon are: T: Physical temperature of the object; ϵ: emissivity of the object; r: reflectivity of the object and t: transmissivity of the object.

2.1.2. X-ray Imaging

X-radiation has a wavelength in the range of 10-0.01 nm ($3{\cdot}10^{16}$-$3{\cdot}10^{19}$ Hz) and enough energy to pass through cloth and human tissues. In addition to cloth penetration, XR imaging provides high image resolution. However, this technology presents some **disadvantages**: low

speed, limitation to very short distances and the health safety concerns it raises because of using ionizing radiation. The natural background X-radiation is too weak to form an image, therefore active imaging is required in both XR imaging modalities: transmission and backscatter X-ray imaging. X-rays are commonly produced by accelerating charged particles.

2.1.3. Infrared Imaging

The Infrared band of the electromagnetic spectrum lies between the SMW and VIS regions, with wavelengths in the range of 0.7-100 μm (see Fig.2.1). The human body emits IR radiation with a wavelength between 3-14 μm hence both active and passive architectures can be used in IR imaging, depending on the considered IR sub-band.

The radiation that is actually detected by an IR sensor depends on the surface properties of the object (ϵ, r, t) and on the transmissivity of the medium (atmosphere). According to the properties of the medium and the spectral ranges of the currently available IR detectors, the IR spectrum is divided into three sub-bands. The limits of these sub-bands are not completely fixed and depend on the specific application. In practice, IR imaging systems usually operate in one of the three following IR sub-bands: the **near infrared** (NIR), **the medium wave infrared** (MWIR) or the **long wave infrared** (LWIR), where the windows of high atmospheric transmissivity are located.

2.1.3.1. NIR: Near Infrared Imaging

As the human body emits IR radiation with a wavelength out of the NIR band (0.7-1 μm) it is necessary to illuminate the body with a NIR source and detect the reflected NIR radiation. So in this case, an **active architecture** is needed. Fig.2.3 (left) shows an image acquired at this band. The images obtained at NIR band are quite similar to the ones acquired at VIS, however they present several advantages: *i*) they are environmental illumination and human body condition invariant, and *ii*) they can provide a good quality vein pattern near the skin surface. The last one is due to two facts: *i*) the incident NIR light can penetrate into the biological tissue approximately 3 mm and *ii*) the reduced hemoglobin in venous blood absorbs more of the incident NIR radiation than the surrounding tissues giving darker contrast. Many biometric research works have been developed using the NIR band [Ferrer *et al.*, 2009; Li *et al.*, 2007]. Face and hand vein pattern recognition are the most important modalities investigated in this band.

2.1.3.2. MWIR: Medium Wave Infrared Imaging

The human body emits IR radiation in this band (3-5 μm) allowing the passive imaging. Therefore, the images obtained in this frequency range show patterns of radiated heat from the body's surface. A comparison between some face images acquired at different IR bands is shown in Fig.2.3. Very few biometric research works have been developed in this band, probably due to the high cost of MWIR cameras. Buddharaju *et al.* [2007] performed face recognition from the

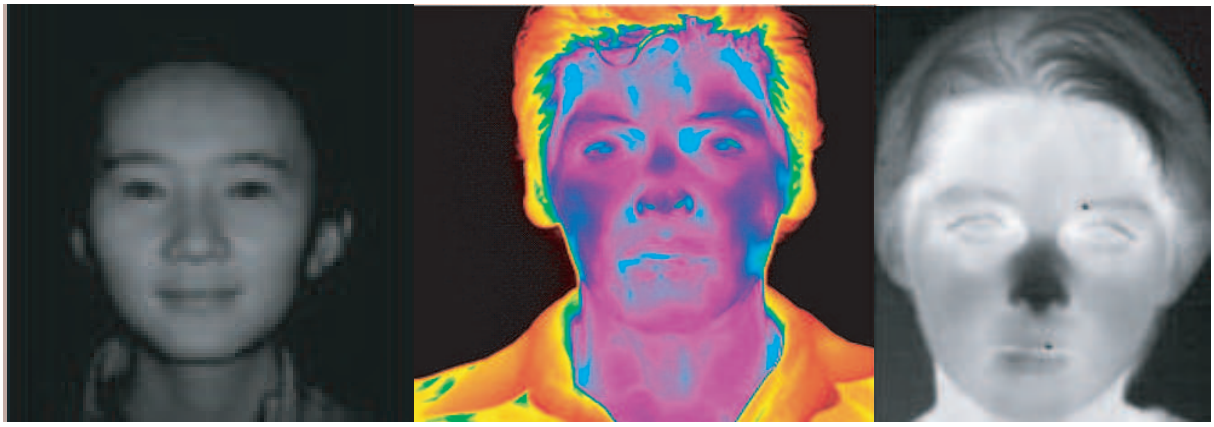

Figure 2.3: *From left to right: Images acquired at a NIR, MWIR and LWIR band. Images extracted from [Buddharaju* et al.*, 2007; Chen* et al.*, 2005; Li* et al.*, 2007]*

thermal imprint of the facial vascular network obtained at the MWIR band. Thermal images of palm dorsum vein acquired in MWIR have been also used to identify individuals Lin and Fan [2004].

2.1.3.3. LWIR: Long Wave Infrared Imaging

Although human body emits IR radiation in both MWIR and LWIR bands, LWIR (8-14 μm) is usually preferred due to: *i*) much higher emissions in it, and *ii*) the low cost of LWIR cameras. No external illumination is required in this band. Body images acquired at LWIR are quite similar to those acquired in MWIR. Both kinds of images are often called *thermograms*. Fig.2.3 (right) shows a face image acquired at this band. Recognition of faces from images obtained at this band has become an area of growing interest [Chen and Jain, 2005; Selinger and Socolinsky, 2004]. However, the algorithms they used do not differ very much from the algorithms used in the VIS band. Works on vein pattern recognition have been developed at this band as well [Wang and Leedham, 2006]. In contrast with NIR; LWIR can only capture large veins, not necessarily at the skin surface since large veins carry a high amount of blood giving a higher temperature. In addition, most of the LWIR images have low levels of contrast and they are sensitive to ambient and body condition.

2.1.4. Millimeter and Submillimeter Wave Imaging

MMW and SMW radiation fill the gap between the IR and the microwaves (see Fig.2.1). Specifically, millimeter waves lie in the band of 30-300 GHz (10-1 mm) while submillimeter waves lie in the range of 0.3-3 THz (1-0.1 mm).

MMW and SMW radiation has the capability of penetration, mainly in nonpolar dielectric materials such as paper, plastics, wood, leather, hair and even dry walls with little attenuation. Clothing is highly transparent to the MMW radiation and partially transparent to the SMW radiation. This transparency is more efficient when working at transparent windows. These

transparent windows are centered at 35, 94, 140 and 220 MHz in the MMW range and at 0.34, 0.67, 1.5, 2, 2.1, 25, 3.4 and 4.3 in the SMW range.

Consequently, natural applications of MMW and SMW imaging include security screening, non-destructive inspection, and medical and biometrics imaging. Low visibility navigation is another application of MMW imaging [Yujiri *et al.*, 2003]. The detection of concealed weapons has been the most developed application of MMW/SMW imaging systems so far, in contrast to the biometrics area, where there are just a few published research works.

Although most of the radiation emitted by the human body belongs to the MWIR and LWIR bands, it emits radiation in the SMW and MMW regions as well . This allows **passive imaging**. However, the sky illumination is a key factor in MMW and SMW passive imaging that makes indoor and outdoor environments to have very different contrast when working with passive systems. This is mainly due to the different variation of temperature between the floor and the sky in outdoors and indoors. While this variation is very large outdoors, it is very small indoors. Moreover, with passive imaging operation indoors, the signal to noise ratio (SNR) of the existing cameras is insufficient for identification (as needed for biometrics). The solutions proposed to overcome this problem are very expensive and difficult to use.

In **active imaging**, the source that illuminates the scene produces much higher power level than the emitted from the scene, so it can be considered as an object at very high temperature. If the source is incoherent and physically large, active imaging is equivalent to passive imaging with the surroundings at very high temperature, and hence results in much greater contrast within the image. If the source is small, active imaging becomes more complicated. In any case, the power level of the radiation source in active imaging strongly affects the detection resolution. In addition to higher resolution than passive imaging, active imaging provides higher SNR, higher signal levels, and the ability to obtain depth information in the scene.

In the following subsections the MMW and SMW will be explained in more detail, showing the difference between passive and active systems.

2.1.4.1. Millimeter Wave Imaging (MMW)

Passive MMW Imaging (PMMW)

There have been many research groups working on passive MMW imaging (PMMW) since its early developments. Most of them have constructed prototype radiometers that work at a frequency range centered at 35 GHz [Sinclair *et al.*, 2002] or at 94 GHz [Howald *et al.*, 2007; Kapilevich *et al.*, 2007; Mait *et al.*, 2009; Sato *et al.*, 2007]. The images obtained with PMMW imaging systems have low resolution compared to VIS and IR images. This low resolution is a consequence of the longer wavelengths used relative to the aperture size of the sensor's collection optics. Further, images acquired indoors will present less contrast than those acquired outdoors, as it is shown in Fig.2.4 (left and center). There are multiple commercial PMMW cameras (e.g. Quinetiq, Brijot, Alfa Imaging, Sago Systems, Millivision, and View Systems).

The applications of most of the cited works are the detection of concealed weapons or vi-

sion under adverse weather conditions. To date, the unique published biometric application of MMW/SMW are the one by Alefs *et al.* [2010] and by Moreno-Moreno *et al.* [2011b] . Specifically, they use a PMMW system, a multi-view stereo radiometric scanner that operates at 94 GHz. The details of mentioned work (the characteristics of the database composed by these images, the approaches followed to perform the biometric recognition and the recognition results) will be briefly presented throughout the document.

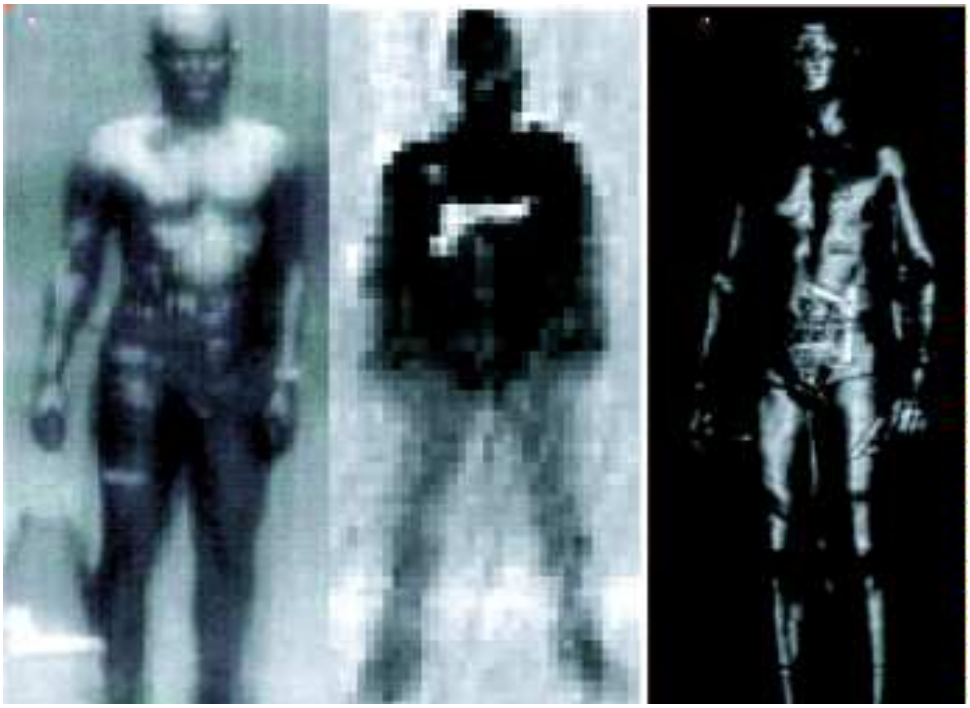

Figure 2.4: *MMW images. From left to right: Outdoors PMMW Image (94 GHz) of a man carrying a gun in a bag; Indoors PMMW image (94 GHz) of a man with a gun concealed under clothing; AMMW image of a man carrying two handguns acquired in 27-33 GHz. Extracted from [Sheen* et al.*, 2001; www.alfaimaging.com; www.vision4thefuture.org]*

Active MMW Imaging (AMMW)

Active MMW imaging (AMMW) has gained more and more attention during the last few years for indoor security applications [Derham *et al.*, 2007; Sheen *et al.*, 2001, 2009; Timms *et al.*, 2007]. Sheen *et al.* [2001] demonstrated an AMMW image operating at 27-33 GHz and good quality images were obtained (see Fig.2.4 (right)). Derham *et al.* [2007] showed the performance of a prototype AMMW imaging system operating at 60 GHz that uses the frequency-encoding technique.Timms *et al.* [2007] developed a 190 GHz active imaging system.

In the active systems, as the image is formed collecting the transmitted and the reflected radiation from the emitting source, the appearance of the images acquired indoors and outdoors is the same (the surrounding temperature does not affect as in the case of PMMW imaging).

An image obtained with AMMW imaging systems is shown in Fig.2.4 (right). The higher

quality of the images acquired with active systems, when compared with PMMW systems, is clearly noticeable (see Fig.2.4 (left and center)) . Again, most of AMMW imaging systems are used as security portals. Some AMMW images are currently available on the market (Agilent and L3-Communications). Agilent's MMW imaging system works at 30 GHz and has a transverse resolution of 1 cm.

2.1.4.2. Submillimeter Wave Imaging (SMW)

The shorter the radiation wavelength is, the better image resolution is available, and hence SMW imaging would provide better resolution than MMW imaging (see Fig.2.1). On the other hand, as the wavelength decreases, the penetration capability decreases. Further, the technology available in the SMW imaging systems is much less mature than the MMW technology [Petkie *et al.*, 2008].

Passive SMW Imaging (PSMW)

In passive SMW imaging (PSMW) the contrast in the image depends on the operation frequency: at frequencies below 0.5 THz it will be dominated by the reflectivity of the items, while at frequencies of 0.5 THz and above, it will be dominated by the emissivity of the objects and their physical temperature (similar to thermography).

Some of the more relevant and recent research works on PSMW imaging include [Luukanen *et al.*, 2006] and [Shen *et al.*, 2008]. Luukanen *et al.* [2006] developed an imaging system working at 0.1-1 THz. Shen *et al.* [2008] performed detection and segmentation of concealed objects in images acquired by the imaging system described in [Luukanen *et al.*, 2006]. They obtain good quality images as it can be seen in Fig.2.5 (left). Fig.2.5 (right) shows another PSMW image of a man with a spanner hidden under his T-shirt (acquired at 1.5 THz [Luukanen *et al.*, 2006]). These two images show that cloth is less transparent to submilliter waves compared to MMW radiation (collar and folds of the weave are visible). A passive system required to penetrate all types of clothing should operate below 0.3-0.5 THz [Appleby and Anderton, 2007; Bjarnason *et al.*, 2004].

The higher resolution of SMW images compared to MMW makes SMW more suitable for biometric recognition applications. However the partial clothing opacity to SMW radiation would hinder the performance of biometric systems. To the best of our knowledge, no biometric works have been performed using PSMW imaging. Regarding commercial PSMW imaging systems, Thruvision currently produces what it seems to be the only commercially available passive THz imaging system [Thruvision].

Active SMW Imaging (ASMW)

Research works on active SMW imaging (ASMW) have only appeared recently [Cooper *et al.*,

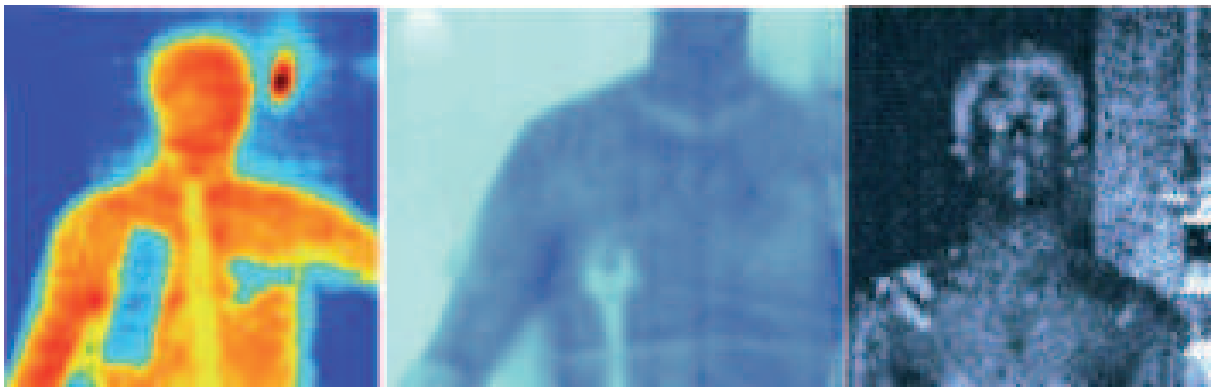

Figure 2.5: *SMW images. From left to right: PSMW image (0.1-1 THz) of a man with concealed objects beneath his jacket; PSMW image of a man with a spanner under his T-shirt; ASMW image of a man hiding a gun beneath his shirt. Images extracted from [Cooper* et al.*, 2008; Luukanen* et al.*, 2008; Shen* et al.*, 2008]*

2008; Lee *et al.*, 2006; Sheen *et al.*, 2009; Tamminen *et al.*, 2008]. Some of them can image a body part at a distance at 0.6-0.8 THz with a spatial resolution of less than 1 cm [Cooper *et al.*, 2008]; Tamminen *et al.* [2008] and, Lee *et al.* [2006] present much better resolution (2mm) working with relatively close targets at 310 GHz ([Tamminen *et al.*, 2008]), or beyond 1 THz ([Cooper *et al.*, 2008]). Finally Sheen *et al.* [2009] developed a prototype system that operates near 350 GHz. Fig.2.5 (right) shows an image acquired at SMW with the active architecture.

Although images acquired at a distance with ASMW imaging systems present not very high spatial resolution, extracting signals from the noisy scene clutter is possible [Cooper *et al.*, 2008]. Furthermore, images acquired from targets near the system present a reasonable resolution for biometric applications, as it happens with fingerprints.

2.2. Shape Matching

Visual information plays an important role in our society. An image has the ability to communicate a complex story or a set of ideas by simply watching to it. There is a growing interest in finding images in large collections, localizing certaing types of objects within images. In order to find an object within the image, it has to be described or represented by certain features. Past work on object recognition has developed the use of two major cues: appearance and shape.

The appearance-based recognition, makes direct use of pixel brightness values.

Shape is an important visual feature and it is one of the basic features used to describe image content. However, shape representation and description is a difficult task. This is mainly due to the loss of one dimension when projecting objects onto a 2-D image plane. As a result, the shape extracted from the image only partially represents the projected object. Adittionaly, the problem worsens as shape is corrupted with noise, defects, arbitrary distorsion and occlusion.

Shape representation generally looks for effective and perceptually important shape features

based on either shape boundary information or boundary plus interior content. According to [Yang *et al.*, 2008], efficient shape features require to possess some requirements such as:

- **identifiability**: similar shapes need to have a feature able to recognize them from other types of shapes.
- **translation, rotation and scale invariance**: the chosen feature needs to be invariant to translation, rotation and scale changes.
- **affine invariance**: when an affine transform is applied to a shape, the 2D coordinates are changed. The shape features requires being as independent as possible to this transformations.
- **noise resistance**: features must be as robust as possible againts noise.
- **occlusion invariance**: when some parts of a shape are occluded by other objects, the feature of the visible part must not change.
- **satistically independence**: if more than one feature is used to represent a shape, they must be statistically independent.

There is a wide variety of techniques to model a shape and different classifications can be found according to different aspects. In [Zhang and Lu, 2004] a classification is exposed. Shape representation can be generally classified into two classes of methods: contour-based methods and region-based methods. The classification is based on whether shape features are extracted from the contour only or are extracted from the whole shape region. Under each class, the different methods are further divided into structural approaches and global approaches. This sub-class is based on whether the shape is represented as a whole or represented by segments.

Yang *et al.* [2008] classifies the techniques according to their processing approaches. It describes in detail the main types of object recognition techniques. We found: one-dimension functions such as complex coordinates, polynomial approximations, spacial features, moments, space-scalars techniques and techniques to project to other domains. Fig.2.6 shows the hierarchy of the classification of shape feature extraction approaches.

Alternatively, shape can be represented by a set of numbers called descriptors. A descriptor attempts to quantify shape in ways that agree with human intuition. Usually, the descriptors are in the form of a vector. Shape descriptors should obey some requirements [Yang *et al.*, 2008]

- **completeness**: the descriptors should be as complete as possible to represent the content of the information items.
- **compact size**: the descriptors should be represented and stored compactly. The size of descriptor vector must not be too large.
- **reasonable computation cost**: the computation of distance between descriptors should be simple so as to reach reasonable computation time.

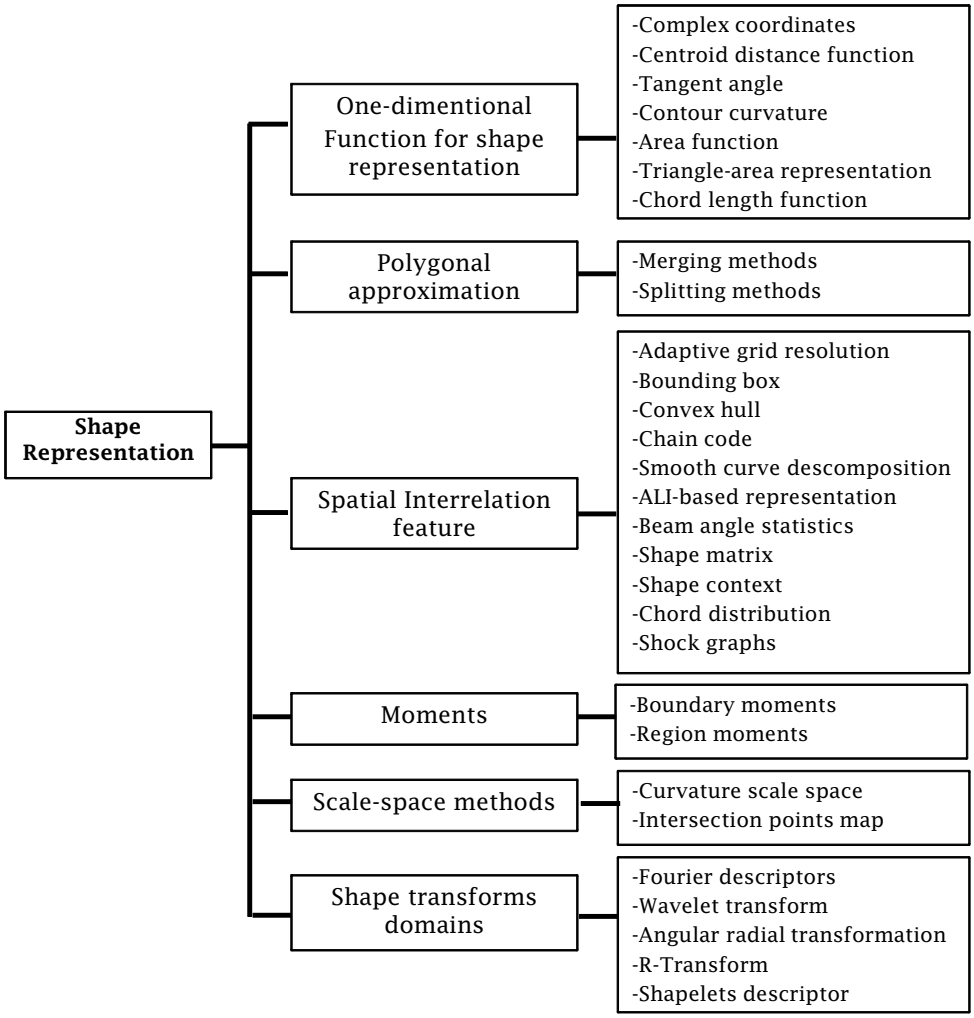

Figure 2.6: *Shape matching classification according to Yang* et al. *[2008]*

The simplest descriptor is a vector of image pixels. However, the high dimensionality of the descriptor results in a high computational complexity for recognition which is not feasible for commercial systems. Mikolajczyk and Schmid [2005], presents a wide study about the different types of descriptors that can be used in the field of object recognition. For instance: distribution-based descriptors, descriptors containing space-frequential informacion, differential descriptors, etc.

Mikolajczyk and Schmid [2005] exposes that in order to solve the multiobject recognition problem; it is desirable to use more than one feature, or a combination between characteristics (color information, texture information, and principal component analysis). This is because it has been proved that there is no single feature that works optimally for all kinds of classes.

The aim of this work consists of building a biometric system using the information of the human contour extracted from images acquired at 94 GHz. In the following chapter, the techniques chosen to build this biometric system for MMW-images will be described in more detail. At the same time, several types of distances to compute the score will be summarized.

Chapter 3

Methods Implemented

In this chapter, we introduce the methods proposed for modeling the silhouettes of people using their contours. As it has been mentioned before, the goal of this Dissertation consists of building a biometric system based on the contour information. To this aim, different techniques are implemented and compared between them in order to discover which configuration optimizes the performance of the system.

Fig.3.1 draws a simple diagram explaining the different stages of the body-shape based biometric system. As can be seen, there are two principal stages: the contour extraction, the parameterization stage and the classification stage.

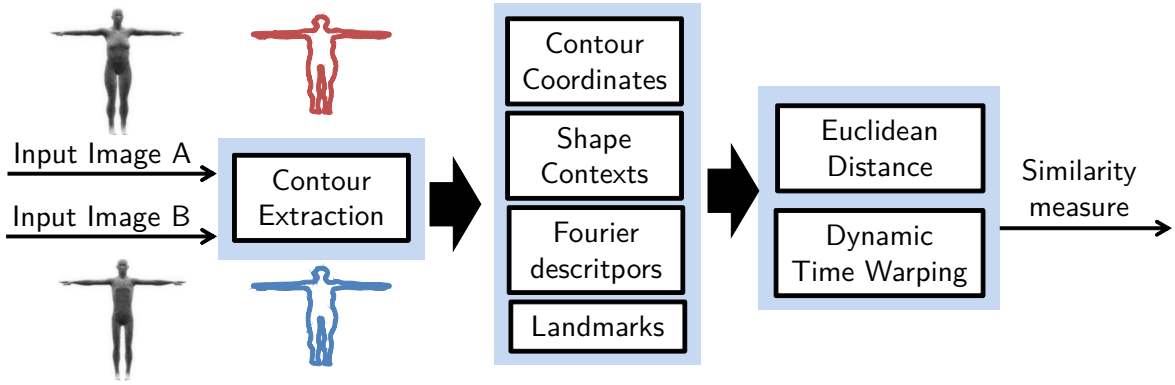

Figure 3.1: *General scheme of the combination of the different techniques that are used in this work*

Within the parameterization and the classification stage, there are several techniques that may be applied. We have selected for the parameterization stage four different approaches: **Contour Coordinates** themselves, **Shape Contexts** (a complex descriptor proposed by Belongie *et al.* [2002]) and using **Fourier Descriptors** of the coordinates [Persoon and Fu, 1977] and **Landmarks** which are a reduced set of points which describe the more discriminative parts of the silhouette.

Regarding the classification stage, two types of distances are employed: the naive approach: **Euclidean Distance** and the **DTW algorithm**, a more complex technique to compute a

similarity between sequences of points proposed by Yasuhara and Oka [1977].

Bellow, we will proceed to outline some of the aforementioned techniques, among them: Dynamic Time Warping, Shape Contexts descriptors, Fourier Descriptors and Landmarks.

3.1. Shape Contexts (SC)

Shape Contexts descriptors were first introduced by Belongie *et al.* [2002]. This technique addresses to describe the feasibility of a specific point by pointing out the relative distance and angle of the rest of the points within a shape. The number of radial bins and theta bins are the main parameters of this descriptor. The shape of an object is represented as a discrete set of points on the contour. A subset of the contour points is selected as centers for computing the shape contexts descriptor, defined as a log-polar histogram. Each point of the shape is situated in its corresponding bin, providing a description of the entire shape relative to the specific point. As a result, the shape contexts descriptor of each point of a shape is fixed to a $(r\_bins * \theta\_bins)$-vector.

For a point p_i on the shape, we compute a coarse histogram h_i of the relative coordinates of the remaining n-1 points of the shape:

$$h_i(k) = \#\{q \neq p_i : (q - p_i) \in bin(k)\} \tag{3.1}$$

The basic idea of shape contexts is illustrated in Fig.3.2, which shows an example of a shape context descriptor for two points in the eigth digit. Note that the log-polar histogram used in this case is a $12*5-length$ vector. Dark colors mean a high density of points within a bin, while ligther colors imply less density of points. In both cases the majority of points are quite distant from the specific point. Regarding the angle distance, in the first case (see Fig.3.2 (a) and (b)) the major density of points relies on the farthest angle distances, while for the second case (see Fig.3.2 (c) and (d)) there are approximately as many points in a medium angle distance as in the far angle distance.

Given two shape contexts, which are histograms, one can measure how likely they come from the same underlying distribution. In order to compute the similarity between two shape contexts, different distance method or standard statistical methods may be applied.

This work attempts to study whether this complex descriptor may improve the performance of the system or not. Once the shape contexts descriptors are computed for all the points describing a contour, DTW algorithm is applied to find the best alignment between them instead of using the contour coordinates.

3.2. Fourier Descriptors (FD)

Although, Fourier descriptors (FD) are a 40-year-old technique, it is still considered as a valid description tool [Yang *et al.*, 2008]. These descriptors are simple to compute and robust

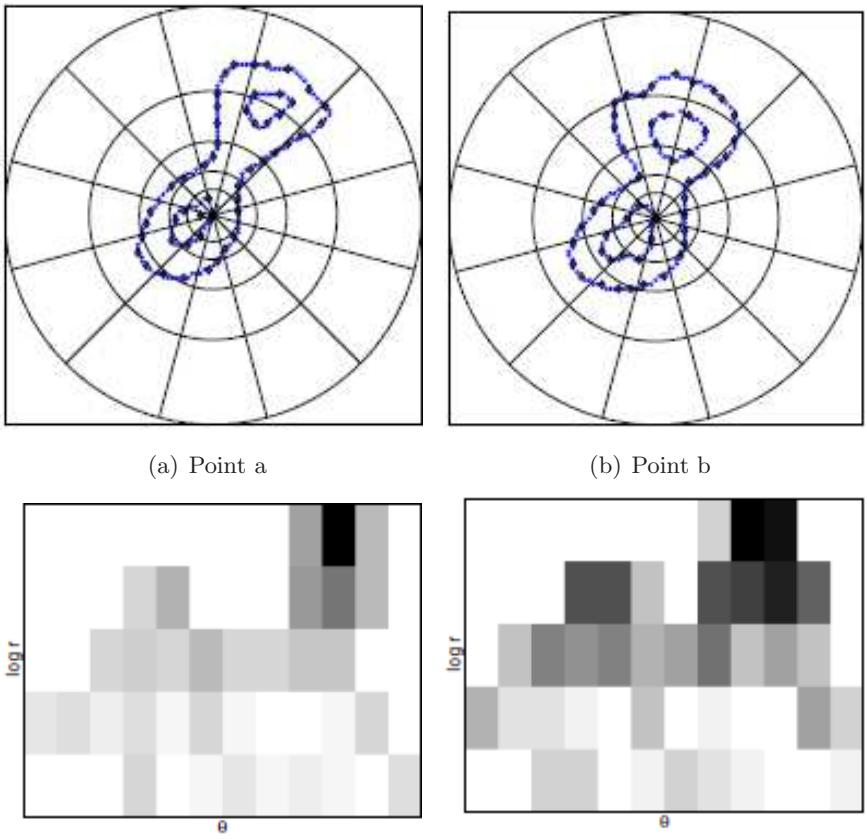

(a) Point a (b) Point b

(c) Histogram point a (d) Histogram point b

Figure 3.2: *Example of the computation of a shape contexts descriptor for two single points within the eight digit. a) and c) represent a point within the eight digit and its respective log-polar histogram; b) and d) for point within the digit and its associated log-polar histogram. Extracted from [Zhang and Malik, 2003])*

against translations and rotations since the effect these transformations cause on the descriptors is completely known. For more details, see [Theodoridis *et al.*, 2010].

First, in order to compute the Fourier descriptors we need to represent the Contour Coordinates as complex numbers (see Equation 3.2). Secondly, we apply the Fourier Transform to the complex numbers to obtain the Fourier description (see Equation 3.3).

Let (x_k,y_k), $K = 0,1,...N-1$ be the coordinates of N samples on the boundary of an image region, see Fig. 3.3. For each pair (x_k,y_k) we define the complex variable:

$$u_k = x_k + jy_k \tag{3.2}$$

For the N u_k points we obtain the DFT f_l

$$f_l = \sum_{k=0}^{N-1} u_k exp(-j\frac{2\pi}{N}lk), l = 0, 1, ..., N-1 \tag{3.3}$$

The coefficients f_l are also known as Fourier descriptors of the boundary. Once the f_l are

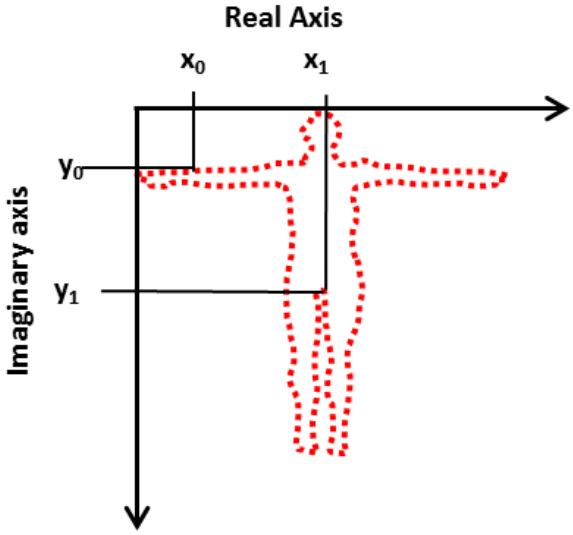

Figure 3.3: *A digital boundary and its representation as a complex sequence. Starting point x_0 and y_0, selected arbitrarily*

available, the u_k can be recovered and the boundary can be reconstructed. The inverse Fourier transform of these coefficients that restores u_k is:

$$u_k = \frac{1}{N}\sum_{l=0}^{N-1} f_l exp(j\frac{2\pi}{N}lk), k = 0, 1, ..., N-1 \tag{3.4}$$

If, instead of using all Fourier descriptors, we use only the first P coefficients in computing the inverse transformation, this is equivalent to setting $f_l = 0$ for $l > P-1$. The result of the inverse transformation is not 100% accurate, but an approximation to u_k:

$$\hat{u}_k = \frac{1}{N}\sum_{l=0}^{P-1} f_l exp(j\frac{2\pi}{N}lk), k = 0, 1, ..., N-1 \tag{3.5}$$

Although only P terms are used to obtain each component of $\hat{u}_k$, k still ranges from *0* to *N-1*. Hence, the same number of points exists in the approximate boundary, but not as many terms are used in the reconstruction of each point. Bearing in mind that high-frequency components account for fine detail, and low-frequency components determine global shape, the discriminatory information of the shape is not lost.

3.3. Landmarks (LM)

This last approach is proposed as a possible feature for the parameterization stage of the system. These landmarks consists of a reduced set of points obtained in the work by Moreno Moreno [2012]. These landmarks were used as reference points from which some of the 21 distance measures were taken. Fig.3.4 depict an example of the situation of these 14 points. In particular,

they try to represent the most singular parts of the people silhouette:

- 1 point describing the top center of the head
- 2 points describing both sides of the neck
- 2 points describing the limits of the hands
- 2 points describing the underarms
- 2 points describing both sides of the waist
- 2 points describing each side of the hip
- 1 point describing the pubis
- 2 points describing the two feet

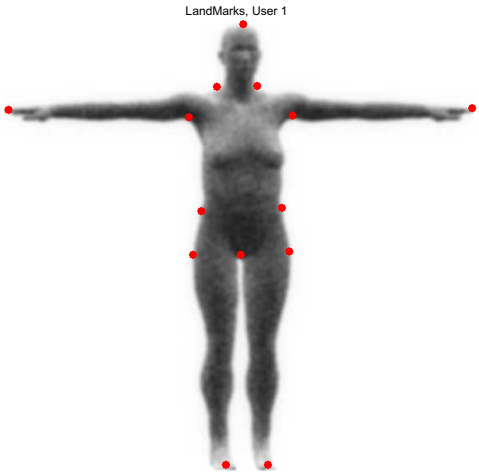

Figure 3.4: *Set of 14 points describing the silhouette of a user 1*

In this work, we aim to use these landmarks as features with the DTW or ED classifier, evaluate the results obtained and compare them with the results achieved with the other approaches.

3.4. Dynamic Time Warping (DTW)

Dynamic Time Warping is an application of Dynamic Programming to the problem of matching time sequences. Yasuhara and Oka [1977] were the first to report its suitability for dynamic signature verification. This Dynamic Programming technique aims to find the best alignment between two sets of points that do not share their dimension (different number of points) minimizing a given distance measure. This algorithm deals with some global and local restrictions

which describes the boundaries of correspondences that may be established between these two sets of points. In the biometric field, it was first used for speech recognition and signature verification [Jain *et al.*, 2002; Kholmatov and Yanikoglu, 2005].

The correspondence may be established by using some specific characteristic of the point. The characteristics that have been used in different experiments of signature recognition [Jain *et al.*, 2002; Kholmatov and Yanikoglu, 2005] are based on local features and global features. The main local features are the coordinates (x,y), difference of coordinates (δx, δy), angle features ($\sin(\alpha)$, $\cos(\alpha)$), absolute and relative speed, gray values, pressure values, etc. The main global features are the number of coordinates, total amount of time, bounding box, number of strokes, etc.

DTW algorithm is useful for our work since this algorithm do not require having sequences with the same dimensionality. The contours extracted from the BIOGIGA images do not have the same amount of points so, in order to compute a similarity measure between sequences of points from different silhouettes, we use the DTW algorithm which obtains a cumulative distance between the Contour Coordinates of two subjects. In Chapter 4, we study the variation in the dimensionality of the contours from the same user and from different users.

3.4.1. DTW Algorithm

In this section, we introduce the DTW algorithm. We base on the work by [Martínez-Díaz, 2008] to explain the details of this algorithm. Let's define two sequences, in this case, the sequences refers to the Contour Coordinates of two people.

$$X = x_1, x_2, ..., x_i, ...x_I$$
$$Y = y_1, y_2, ..., y_i, ...y_J$$

and a distance measure as

$$d(i,j) = ||x_i - y_j|| \tag{3.6}$$

between sequence samples. A warping path can be defined as

$$C = c_1, c_2, ..., c_k, ..., c_K \tag{3.7}$$

where each c_k represents a correspondence *(i,j)* between samples of X and Y. The initial condition of the algorithm is set to

$$g_1 = g(1,1) = d(1,1)w(1) \tag{3.8}$$

Where g_k represents the accumulated distance after k steps and *w(k)* is a weighting factor that must be defined. For each iteration, g_k is computed as

$$g_k = g(i,j) = \underset{c_{k-1}}{min}[g_{k-1} + d(c_k)w(k)] \tag{3.9}$$

until the *(I'th)* and *(J'th)* sample of both sequences respectively is reached. The resulting normalized distance is

$$D(X,Y) = \frac{g_k}{\sum_{k=1}^{K} w(k)} \tag{3.10}$$

The weighting factors w_k are defined in order to restrict which correspondences among samples of both sequences are allowed. In Fig.3.5 (left), a possible definition of w_k is depicted. In this case, only three transitions are allowed in the computation of g_k.

In Fig.3.5 (right), an example of point correspondences between two signatures is depicted to visually show the results of the elastic alignment.

The algorithm has been further refined for signature verification by many authors [Kholmatov and Yanikoglu, 2005; Martens and Claesen, 1997; Sato *et al.*, 2007]. Although the DTW algorithm has been replaced by more powerful ones such as HMMs or SVMs for speech applications, it remains a highly effective tool for signature verification as it is best suited for small amounts of training data, which is the common case in signature verification.

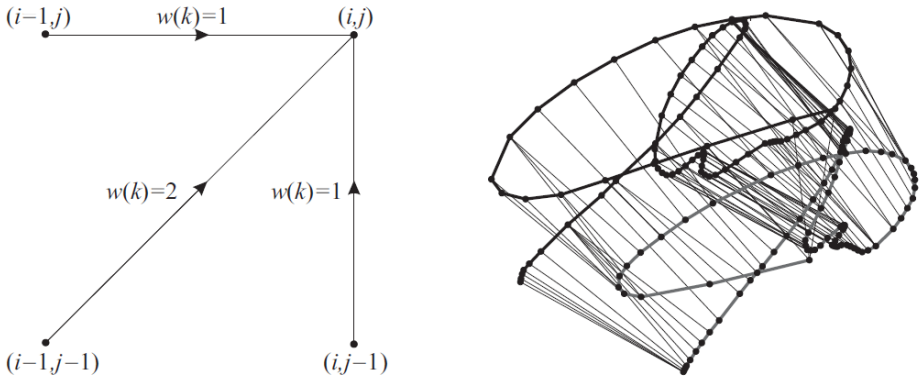

Figure 3.5: *Example of symmetrical weighting factors $w(k)$ for Dynamic Time Warping (left). Example of point-to-point correspondences between two genuine signatures obtained using DTW extracted from [Martínez-Díaz, 2008] (right).*

In this work, DTW is used to obtain a cumulative distance between two strings of coordinates that is known to be minimal. Equation 3.11 shows the transformation of this minimal distance into a matching score where K is a normalization factor that takes into account the number of aligned points between two sequences.

$$score = \exp^{\frac{-dist}{K}} \tag{3.11}$$

Chapter 4

Experimental Framework

The lack of databases in the MMW band due to the privacy concerns the MMW body images present hinders the acquisition of images in this band. To the best of the author's knowledge, there are few databases of MMW body images. In particular, we are aware of the **TNO database**, which was created by Alefs *et al.* [2010] and has captured real images from people bodies and the **BIOGIGA database**, which is a synthetic database developed by Moreno-Moreno *et al.* [2011a] which simulates the effect of the MMW band. Due to the privacy concerns that the **TNO database** presents, we decide to use the **BIOGIGA database**. A more complex description about the BIOGIGA database is given throughout this chapter.

This chapter also covers the procedure to extract the contours from the images and the experimental procedure carried out to analyze the performance of the different approaches described in Chapter 3.

4.1. BIOGIGA Database

The corpus of the BIOGIGA database consists of synthetic images at 94 GHz of the body of 50 individuals: 25 males and 25 females with ages ranging from 15 to 55 years old. The corporal models were previously generated using the software MakeHuman [2011] based on body measurements taken from the subjects. Then, these models were imported to Blender [2011], which simulates the effect of the 94 GHz radiation over the human models. The images are the result of simulations carried out on corporal models at two types of scenarios (outdoors and indoors) and with two kinds of imaging systems (passive and active, see subsection 2.1.1 for more details).Then, for each user, the database has four sets of images, each of them simulated by:

- A passive system outdoors (PO).
- A passive system indoors (PI).
- An active system outdoors (AO).

- An active system indoors (AI).

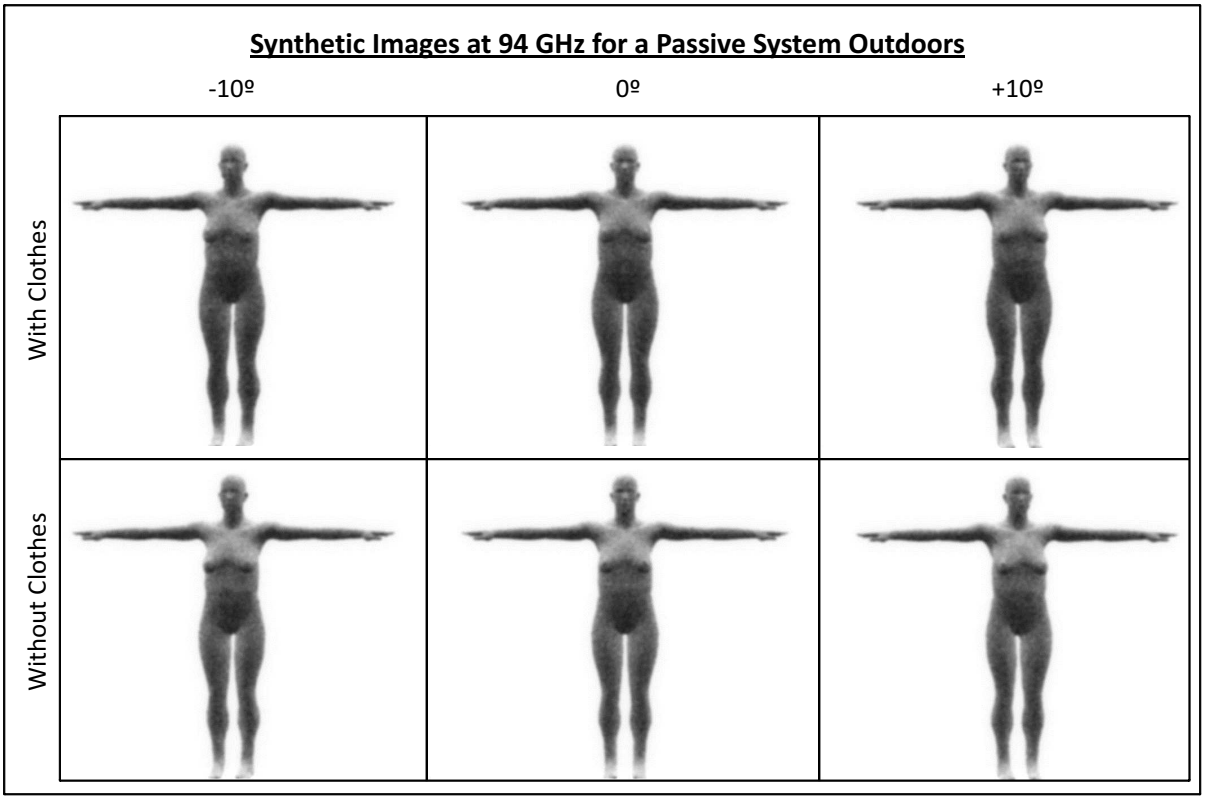

Figure 4.1: *Synthetic images acquired at 94 GHz and extracted from the BIOGIGA database [Moreno-Moreno* et al.*, 2011a]. The six images represent the user_id=1 user with a passive system and outdoors. The figure shows the three different camera angles, and images with clothes and without clothes*

In each of these four scenarios, six different images from each user are taken. Three of them are simulated with clothes, and the other three are simulated without clothes to analyze the effect of clothing and have some variability between the images of the same person. For this, three angles between the subject and the camera were considered, having images with -10, 0 and +10 degrees. Therefore, the BIOGIGA database acquires six images per user and per scenario. So, finally, we have 6 images * 50 users * 4 scenarios = 1200 images

In this Dissertation, only passive images at outdoor scenarios are considered (PO). We choose this subset of the database due to the more similarity of this subset with the TNO database and its major resolution. This subset of the database is comprised of 50 subjects, with 6 images per user, making a total of 300 images. Fig. 4.1 shows an example of the images from a single subject of the database with passive system and outdoors scenarios. As it can be seen, images with and without clothes are very similar since the 94 GHz band is transparent to clothes; however, the pixel intensity is a bit darker in the images with clothes and small parts of the clothes are still noticeable in the waist and neck.

Further information about the description of the generation of the BIOGIGA database can be found in [Moreno Moreno, 2012; Moreno-Moreno *et al.*, 2011a].

4.2. Preprocessing Steps: Contour Extraction

The extraction of the contours is obtained as follows. The first step consists of binarizing the images, that is, separate the background from the body. A characteristic of the images simulated by passive systems is the different grey level they present in different parts of the body. For instance the abdomen is much darker than the feet. This fact worsens the segmentation process. This problem is overcome performing the segmentation in two steps: *i)* border detection and *ii)* morphological detection.

A Canny border detector (whose parameters are previously tuned) is first applied to the image. After that, various morphological operations are conducted on the resulting border image. These morphological operations consist of closing operations with different structural elements in different areas of the image (head, arms, from arms to calf, and feet). Finally, another set of morphological closing removes spurious irregularities, and obtains the final contour of the human body, which is used in the following experimental sections. Fig.4.2 shows an example of the process of segmentation and contour extraction.

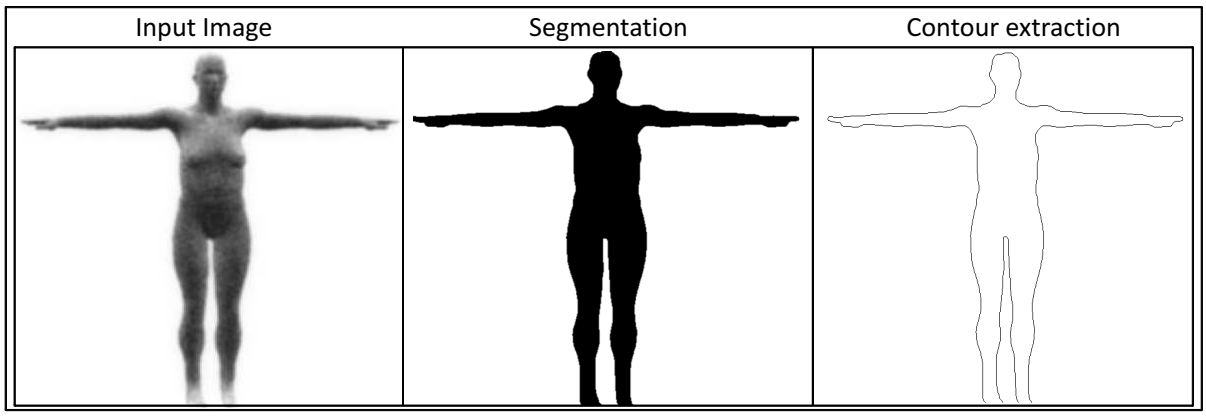

Figure 4.2: *Main steps followed in our system to extract the contour. From left to right: Original image (of a subject with clothing and a camera angle of -10 degrees), segmented image, contour extraction.*

This step was based on the preprocessing stage made in [Moreno Moreno, 2012], but it was necessary to retune the parameters so as to obtain contour sequences valid for the purpose of this work.

4.3. Experimental Framework

In this work, we use protocols in the form of $Px : y$. where the x refers to the number of training images considered per user, and y stands for the number of test images per user. The training images are the ones that the system previously has of each subject and are used to enroll the user into the system, while the test images are the ones given by the user when he or she tries to be accepted by the system.

Taking this into account, two different kinds of protocols are selected: those which use **three**

images as test images, and those which use just one image as test image. From the first type of protocols we have: *i)* protocol 1:3, *ii)* protocol 2:3 and *iii)* protocol 3:3 and from the second type of protocols we have: *i)* protocol 1:1, *ii)* protocol 2:1 and *iii)* protocol 3:1. The reason of using the first type of protocols relies on the interest of having the same experimental framework than the previous work developed by Alefs *et al.* [2010] and Moreno-Moreno *et al.* [2012].

It is worth noting that, in the experiments, all the training images are images simulated with clothes, and the test images without clothes. This configuration is made in order to have the most challenging scenario with severe mismatch between enrollment and testing regarding clothing. The configuration for each protocol is as follows:

- P1:3, train (cr_*), test: (sr_a, sr_b, sr_c)
- P2:3, train (cr_*, cr_*), test: (sr_a, sr_b, sr_c)
- P3:3, train (cr_a, cr_b, cr_c) test: (sr_a, sr_b, sr_c)
- P1:1, train (cr_*), test: (sr_*)
- P1:2, train (cr_*), test: (sr_*, sr_*)
- P1:3, train (cr_*), test: (sr_a, sr_b, sr_c)

Where cr_* stands for images with clothes for the three angles between subject and camera (-10, 0 and 10); sr stands for images without clothes and a, b, c refers to every single camera angle. We have to bear in mind that, when we have 2 or 3 images for training or testing, the fusion of the information contained in the images is carried out at the **score-level**, i.e., all single comparisons between training and test are done image by image, and then the scores are fused using a sum rule. This is mainly due to the fact that contours **do not have the same dimensionality** in all cases, so it is unfeasible to make the fusion at the feature-level.

A major issue to bear in mind relies on the importance of having contours of the same size or not. Since the database contains six different images per individual, every single contour obtained from its respective image has a number of coordinates that do not necessarily coincide with the number of coordinates of the remainder images from the same subject. The same happens when comparing contours from images from different subjects.

Fig.4.3 shows some examples of histograms of dimensionality of the images for single users. As can be observed, the variation between the same subjects differs in 20-30 points approximately. Apart from the **intra-person** variability, there is also a large **inter-person** difference regarding the size of contours belonging to different subjects. From Fig.4.4 can be seen that dimensionality of the contours ranges from 2500 to 3100 points approximately.

In some experiments of this work the contours are normalized (specified in the name of the experiment as **NormS**), that is, all the contours of all the images of the database are **truncated** or **interpolated** to the medium amount of points of all the contours. If the original contour has fewer points than the average, an interpolation is carried out while a truncation is computed

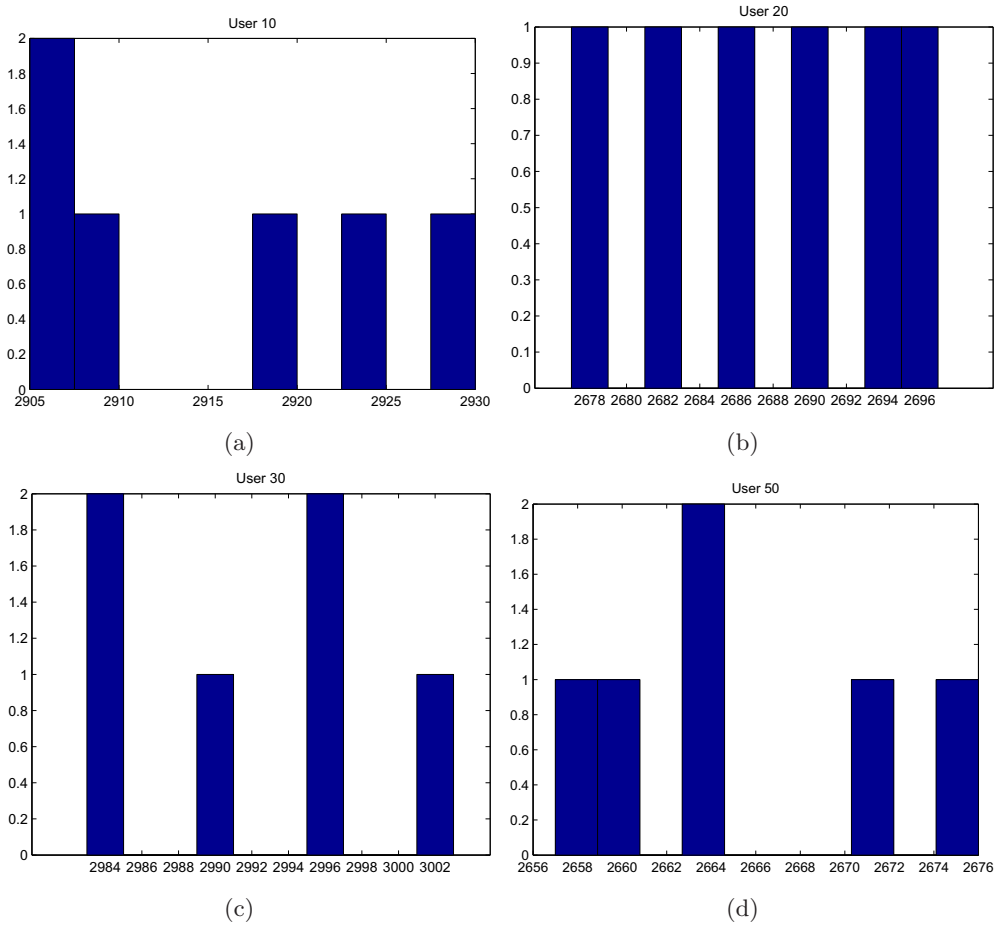

Figure 4.3: *Histogram of the dimensionality of the contours for single users: user_id 10 (a), user_id 20(b), user_id 30(c) and user_id 50(d)*

otherwise. In other experiments, the contour of each single image remains with its original size (specified in the name of the experiment as **MeanS**). If we reduce the dimensionality of the contours and we want to have MeanS contours, the original size of the contours is not maintained. In this case, a subsampling operation is carried out so as to have a number of coordinates whose average is the desired resolution.

The last part of this chapter describes the experiments carried out in this paper. The objective of these experiments is to find the combination of features and classifiers that optimizes the performance of the system bearing in mind also the computational cost. The simulations fulfilled combine the different type of features which can describe the silhouette of the person: Contour Coordinates (CC), Shape Contexts (SC), Fourier Descriptors (FD) and the Landmarks (LM) with the two classifiers proposed in the work: Euclidean Distance (ED) and Dynamic Time Warping algorithm (DTW):

- **CC ED**: Contours Coordinates using Euclidean Distance
- **CC DTW**: Contours Coordinates using Dynamic Time Warping.

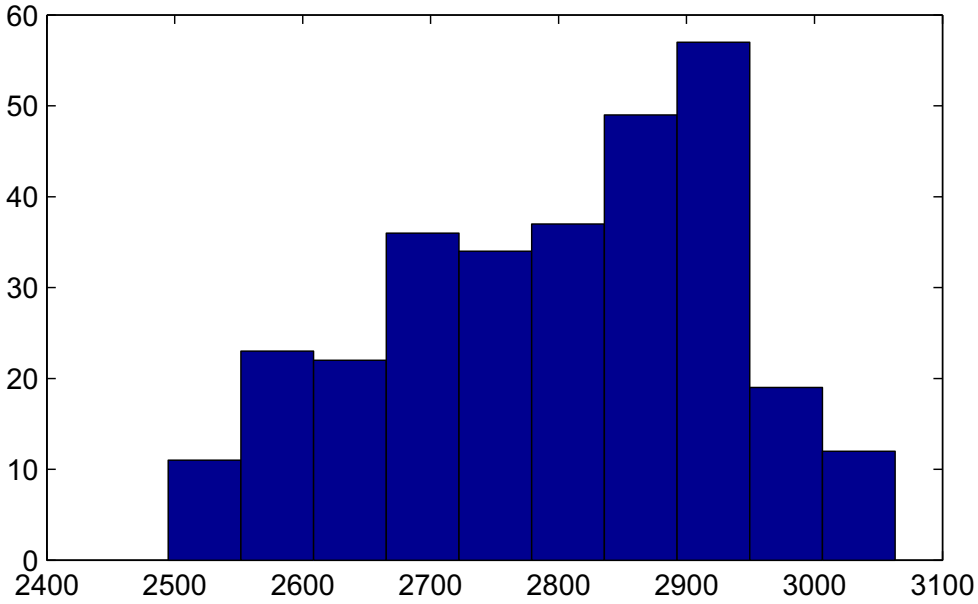

Figure 4.4: *Histogram of the dimensionality of the contours for all the users*

- **CC DTW**: Contours Coordinates using Dynamic Time Warping.
- **SC DTW**: Shape Contexts using Dynamic Time Warping.
- **SC ED**: Shape Contexts using Euclidean Distance.
- **FD DTW**: Fourier Descriptors using Dynamic Time Warping.
- **FD ED**: Fourier Descriptors using Euclidean Distance.
- **LM DTW**: Landmarks using Dynamic Time Warping.
- **LM ED**: Landmarks using Euclidean Distance.

So, to achieve the aforementioned goal, we need to explore the capability of the different features proposed and the different classifiers, the effect of normalizing the contours and the influence of the resolution of the contours. Finally, results achieved here are compared to the results from Moreno-Moreno *et al.* [2012].

4.4. Performance Evaluation

The evaluation of the performance of the system is done through well-known quantitative measures, obtained from experiments, that reveal how well the system works and allow to compare its performance with the performance of other biometric systems [Jain *et al.*, 1999]. When working in verification mode the main metrics used to quantify the performance of the biometric system are:

- **False-Rejection Rate, FRR**: reflects the probability that a genuine user is rejected by the system.
- **False-Acceptance Rate, FAR**: represents the percentage of users that have been falsely accepted as genuine user.
- **Equal Error Rate, EER**: is the point at which FAR = FRR, and gives a measure of the system performance: the lower the EER, the better the performance.
- **Error Detection Trade Off, DET**: Draws the representation of the FAR curve against FRR curve. It is considered as an alternative measure to evaluate the performance of the biometric system.

Note that EER and DET measures are obtained from the FRR and FAR. For the experiments carried out in this work, results are presented in the form of DET Curves and Equal Error Rates , EER. As it has been outlined in Section 1.1, biometric systems can operate in two modes: verification mode and identification mode. In this Dissertation, only verification results are presented.

Chapter 5

Experimental Results

The experimental results of this work are covered in this chapter. Here, we have carried out different experiments with the objective of extracting a reliable conclusion regarding the feasibility and the performance of the system with the different features and classifiers proposed in Chapter 3.

In particular, this chapter is organized as follows. First of all, results are presented according to the features used, that is, first results based on Contour Coordinates are depicted and then results based on Shape Contexts, Fourier Descriptors and Landmarks.

In each case, a deep study of the technique is accomplished to get conclusions about the type of classifier (DTW or ED), the type of normalization (MeanS or NormS) and the dimensionality of the features that optimizes the performance of the system (2800, 1000, 500, 200, 100 points).

All results are presented following the experimental framework described in Section 4.3.

5.1. Contour Coordinates

In this experiment we analyze the performance of a system based on coordinates of the contour. Several classifiers are studied with these features: DTW and ED. In Section 5.1.1 results of the naive system based on Contour Coordinates and ED are presented while results of the system based on Contour Coordinates and DTW are presented in Section 5.1.2.

5.1.1. Contour Coordinates with ED

This is the baseline configuration of our system. In this case, the Contour Coordinates are used as the features of the system and then the Euclidean Distance is used to measure the performance of the system. The results obtained with this configurations are drawn in Table 5.1. As can be seen, different resolutions of the contour are evaluated ranging from 200 points to approximately the original size of the contour: 2800 points.

Note that in this case, only NormS contours can be used, as the Euclidean Distance algorithm requires sequences of the same length. Results are presented for all the protocols defined in

section 4.3. From Table 5.1, we conclude that a change in the resolution of the contour does not entail an improvement of the system. The best configurations of protocols are in order: 3:3, 2:3, 1:3, 3:1, 2:1 and 1:1. However, we have to bear in mind that protocols using 3 images as test images are not so realistic. Protocol 3:1 is the most suitable protocol to develop in practical environments.

Table 5.1: *EER results using the coordinates of the contours as features and ED as classifier changing the resolution of the contour for protocols 1:3, 2:3, 3:3, 1:1, 2:1 and 3:1*

CC ED	EER for protocols: 1:3, 2:3, 3:3, 1:1, 2:1, 3:1					
Experiment	1:3	2:3	3:3	1:1	2:1	3:1
CC 200 NormS ED	5,33%	5,33%	4,85%	9,28%	8,22%	7,55%
CC 500 NormS ED	5,33%	5,33%	4,89%	9,33%	8,22%	7,67%
CC 1000 NormS ED	5,33%	5,33%	4,89%	9,33%	8,22%	7,67%
CC 2800 NormS ED	5,33%	5,33%	4,89%	9,33%	8,22%	7,67%

5.1.2. Contour Coordinates with DTW

In this section we implement a system that uses Contour Coordinates as features and the DTW algorithm as the classifier. As we have contours that do not have the same amount of points (referred in the algorithm as MeanS contours), we need to use an algorithm capable of finding a correspondence between two sequences of points with different resolution. This algorithm is the Dynamic Time Warping. With some initial restrictions, this algorithm is able to reach an alignment between pairs of points with a minimum distance.

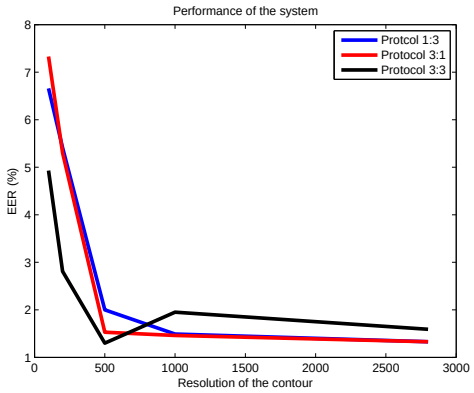

Figure 5.1: *Performance of the system for different contour resolution: 2800, 1000, 500, 200, 100*

Results of the system based on contour coordinates and DTW are depicted in Table 5.2. In

Table 5.2: *EER results using the coordinates of the contours as features and DTW as classifier changing the resolution of the contour and Normalizing its size or not for protocols 1:3, 2:3, 3:3, 1:1, 2:1 and 3:1*

CC DTW	EER for protocols: 1:3, 2:3, 3:3, 1:1, 2:1, 3:1					
Experiment	1:3	2:3	3:3	1:1	2:1	3:1
CC 100 MeanS DTW	6,66%	5,60%	4,93%	14,22%	10,07%	7,33%
CC 100 NormS DTW	6,66%	3,23%	2,00%	10,62%	7,75%	6,00%
CC 200 MeanS DTW	5,41%	4,46%	2,81%	10,44%	7,11%	5,30%
CC 200 NormS DTW	5,33%	4,66%	3,22%	10,07%	6,89%	5,33%
CC 500 MeanS DTW	2,00%	1,18%	1,30%	10,23%	6,37%	1,53%
CC 500 NormS DTW	2,00%	2,00%	2,00%	10,02%	6,00%	2,00%
CC 1000 Means DTW	1,49%	1,49%	1,95%	10,31%	6,66%	1,46%
CC 1000 NormS DTW	2,00%	2,00%	2,00%	9,33%	6,42%	2,00%
CC 2800 MeanS DTW	1,33%	1,23%	1,59%	10,06%	6,66%	1,33%
CC 2800 NormS DTW	1,33%	1,17%	1,51%	9,89%	6,78%	1,33%

this table, we also study the effect of varying the resolution of the contour from 2800 points (the original size of the contour) to 100 points. This reduction is accomplished to discover how many points are really needed to represent accurately the human contours.

According to these results, we conclude that the resolution of the contour is essential to achieve a good performance of the system. As can be seen from all the columns from Table 5.2, as the resolution of the contour decreases, the performance of the systems worsens. In fact, the average relative improvement between the worst (CC 100 MeanS) and the best scenario (CC 2800 Means) is about $76,16\%$ for protocol *x:3* and 48.33% for protocol *x:1*.

Fig.5.1 represents the EER against the resolution of the contour for protocols 1:3, 3:1 and 3:3. We observe, that in order to obtain EER results below the 2%, we need to work with contours with more than 500 or 1000 points. However, if we desire to obtain the best performance possible, we need to work with the higher resolution of the contour, 2800 points. Table 5.2 shows through a color code how these results worsen as the resolution decreases. The darker red colors means a low performance of the system while the darker green colors shows a high performance of the system. For instance when we use the highest resolution of the system, that is 2800 points, and protocols 1:3 or 3:1 we obtain the best EER rates: 1.33%. On the other hand, with contours with poor resolution, such as the case of 100 points, we obtain low EER rates as $10,07\%$ for protocol 2:1 and $14,22\%$ for protocol 1:1.

From these results we also study the influence of normalizing the contour, NormS, or having contours from the same subject with different size (different size, but with a short variation of points between them, MeanS (see Section 4.3 for more details). From the table, we conclude that for contours with the higher resolution such as the case of 2800 points, there is no appreciable improvement between NormS and MeanS contours. When we use contours with 1000 points or 500 points, the majority of protocols do show a little but sufficient variation of performance bewteen NormS and MeanS contours. On the other hand, in the majority of cases of the smaller resolutions, we observe that there is a small variation between MeanS and Norms results or for other protocols, we obtain better results using NormS contours. However, we need to focus on applying NormS or MeanS for the resolution of contour that gets best results which is the CC-2800 resolution. In this particular case, using NormS contours or MeanS contours do not change sufficiently the results.

DET curves for this experiment are depicted in Fig. 5.3 (at the end of this chapter) and help us to have a more reliable vision of the performance of the different configurations. There are six curves, one for each protocol described previously. Comparing the results from the different protocols, we can see how all the DET curves approach the origin when more data is used for the training stage. The best protocols are the ones that use a larger number of images in the training stage: protocols 3:3 and protocols 3:1. It is worth noting that in the case of protocol 3:3 the number of scores is smaller compared to the other protocols, making more difficult to draw an accurate DET curve. For instance in this case, the configuration with the best EER according to Table 5.2 is the CC-500 MeanS DTW. However, we observe from Fig.5.3(e) that for the limit values of FAR and FRR of $0,5\%$ we have a corresponding value of FRR and FAR of 2% for the CC-2800 NormS DTW respectively. For the case of CC-500 MeanS DTW, however, for the limits values of FAR and FRR of $0,5\%$, we have a corresponding value of 6% of FRR and 2% of FAR respectively. Therefore, we understand that although the EER results of the CC-500 MeanS DTW curve are slightly better, the CC-2800 configurations are more suitable for the system.

Comparison between DTW and ED

Comparing the last row of Table 5.1 with the last row of 5.2, we confirm that using DTW results in a higher performance of the system, having an average relative improvement of $74,10\%$ for protocols *x:3* and $31,39\%$ for protocols *x:1*. This is mainly due to the capability of the DTW algorithm to find the best alignment between two sequences of points, in this case, between two sequences of Contour Coordinates.

There is also a huge difference regarding the computational cost of both classifiers. The computational time involved in the DTW algorithm is at least 5 times the computational cost involved when applying the ED algorithm.

5.2. Shape Contexts

In this section we evaluate the performance of a system based on Shape Contexts. As it has been described in section 3, Shape Contexts are complex descriptors of the shape that describe each point within the shape with a log-polar histogram. In this specific case, the Shape Contexts approach was set with a log-polar histogram of 12 bins of radial distance and 5 bins of angle distance (it has been proved its good results in [Belongie *et al.*, 2002]), resulting a vector of 60 components for each point of the contour. Different resolutions of the contours are considered and both classifiers DTW and ED are studied. In the last part of the section a brief analysis of the parameters of the Shape Contexts (described in section 4.3) is carried out.

5.2.1. Shape Contexts with DTW

The experiments carried out in this section use Shape Contexts as features and DTW as classifier. It is worth noting that in this case the score of DTW is computed as following:

$$score = -\frac{DIST}{K} \tag{5.1}$$

The exponential is not applied as in section 5.1.2, because Shape Contexts turn out to provide much better results without applying the exponential function. We study SC with resolutions which range from 200 points to 2800 points being in this case always normalized to the same size, NormS.

Results are depicted in Table 5.3. As we can observe, as the resolution decreases, results worsen in the majority of cases. For example, the average relative improvement between the SC 2800 configuration and the SC 200 configuration is about $16,28\%$ for protocols *x:3*,and $45,40\%$ for protocols *x:1*. The same colors code is applied than in section 5.1.2.

If we compare the SC 2800 configuration from Table 5.3 with the CC 2800 NormS configuration from Table 5.2, we observe that for protocols *x:3* we obtain an average relative improvement of $33,17\%$ between applying CC instead of SC. However for protocols *x:1*, applying SC yields an average relative improvement of $39,60\%$ with respect to the CC features.

5.2.2. Shape Contexts with ED

Only one case of Shape Contexts using ED classifier is studied. In this case, we use the best resolution of points: 2800. As can be seen from the last row of Table 5.3, using DTW algorithm improves the EER of the system for all protocols. When using DTW compared to using ED, the relative improvement of the system on average is of $76,15\%$

The computation cost invested when we work with SC as features increases due to the huge dimensionality of each vector, which needs $r\_bin * theta\_bin * N$ values to build the model of each user. This yield an increase of the computational cost that is magnified even more when applying the DTW algorithm. In particular, the computation cost involved in an algorithm

Table 5.3: *EER results using Shape Contexts as features and ED and DTW as classifier changing the resolution of the contour for protocols 1:3, 2:3, 3:3, 1:1, 2:1 and 3:1*

SC DTW	EER for protocols: 1:3, 2:3, 3:3, 1:1, 2:1, 3:1					
Experiment	1:3	2:3	3:3	1:1	2:1	3:1
SC 200 NormS DTW	3,91%	2,00%	2,00%	10,66%	6,23%	4,66%
SC 500 NormS DTW	2,38%	2,00%	2,00%	9,84%	5,77%	4,00%
SC 1000 NormS DTW	2,00%	2,66%	2,00%	9,57%	5,04%	4,00%
SC 2800 NormS DTW	2,00%	2,00%	2,00%	6,09%	3,33%	2,48%
SC 2800 NormS ED	10,00%	8,66%	9,18%	16,26%	15,11%	13,25%

based on SC and DTW may increase the computation cost of an algorithm based on SC and ED at least ten times.

5.2.3. Studying Shape Contexts

In this last part of the section, we study the results obtained when different parameters of Shape Contexts are changed. Specifically, the parameters we study are the number of radial bins (R_bins), the number of theta bins (R_theta), the relative distance from the point to the first radial bin (R_inner) and to the last radial bin (R_outer). In all cases, we use the higher resolution of points, that is, 2800 points. Table 5.4 explains the different combinations of parameters and the results obtained, being SC0 the reference configuration that are studied. Note that R_theta is set to 12 and R_inner is set to 1/8 in all cases.

As can be seen, using less radial bins such as SC1 which uses 3 bins, results in worst performance. Experiment SC2 uses 10 bins, and these results are slightly better than the SC0 results (mainly for protocols 1:1, 2:1 and 3:1) having an average relative improvement of 12.15%. SC3 and SC4 study whether enlarging R_outer parameter results in better performance of the system or not. We observe from rows fourth and fifth of Table 5.4 that the performance of the system on average are quite similar to the results obtained with SC0. We conclude from this evaluation that the best way to improve the results using SC is using a larger number of radial bins.

5.3. Fourier Descriptors

In this section, we analyze the system based on Fourier Descriptors. In this case, both classifiers DTW and ED are used. Contours may be NormS and MeanS. To carry out this study we use a resolution of 2800 points.

Table 5.4: *EER results of the different configuration of Shape Contexts using DTW in all cases for protocols 1:3, 2:3, 3:3, 1:1, 2:1 and 3:1 with R_theta=12 and R_inner=1/8 for all cases*

SC			EER for protocols: 1:3, 2:3, 3:3, 1:1, 2:1, 3:1					
EXP	R_bins	R_outer	1:3	2:3	3:3	1:1	2:1	3:1
SC 0	5	2	2,00%	2,00%	2,00%	6,09%	3,33%	2,48%
SC 1	3	2	5,60%	4,00%	4,00%	14,00%	9,04%	6,00%
SC 2	10	2	2,00%	2,00%	2,00%	5,65%	3,00%	2,40%
SC 3	5	4	2,00%	2,00%	2,00%	6,22%	3,11%	2,66%
SC 4	5	8	2,00%	2,00%	2,00%	6,72%	3,18%	2,00%

It is worth noting that, in order to apply DTW and ED algorithm, we need to work with the module of the descriptor. Besides, when using DTW algorithm, the score is computed without the exponential as in section 5.2.1.

From Table 5.5, we observe comparing the first and second row that when using the DTW algorithm, results improve with MeanS contours. This is mainly due to the larger number of possible alignments between pair of points when using MeanS contours. However, using MeanS or NormS makes no important difference when using ED classifier.

When comparing the first and third row of Table 5.5, we observe that in the majority of cases there is not any considerable difference of results. In fact, the average EER for each row is $4,39\%$ and $4,33\%$ respectively. So, taking into account these results and the fact that the computation cost of applying DTW algorithm is quite higher than applying the ED, we conclude that in this case, using DTW with Fourier Descriptor as features is not worthwhile.

Table 5.5: *EER results using Fourier Descriptor as features and DTW and ED as classifiers for protocols 1:3, 2:3, 3:3, 1:1, 2:1 and 3:1*

FD	EER for protocols: 1:3, 2:3, 3:3, 1:1, 2:1, 3:1					
Experiment	1:3	2:3	3:3	1:1	2:1	3:1
FD 2800 MeanS DTW	3,30%	3,33%	4,00%	5,33%	5,29%	5,14%
FD 2800 NormS DTW	4,28%	4,95%	5,55%	6,8481%	6,88%	7,33%
FD 2800 NormS ED	2,43%	3,33%	4%	5,61%	5,40%	5,22%

5.4. Landmarks

The last experiment aims to evaluate how efficiently can be a system which describes the subjects with a few points. These points specify the position of certain parts of the silhouette such as the top central point of the head, arms, feet, hips, **key points of the silhouette**. Specifically, we have used 14 points extracted from the work by [Moreno Moreno, 2012] and described briefly in section 4.3. Table 5.6 presents the results obtained with these set of points when using either DTW or ED classifiers. From these results we conclude that using a vector with a dimensionality quite shorter than the vectors used in any of the previous sections of this chapter, produce results comparable to the rest of experiments. In particular, ED classifiers produce better results than the DTW algorithm. In fact, the use of the DTW algorithm for this reduced amount of points is not worthwhile.

However, it is worth noting that this database is ideal since is synthetic and the resulting images do not present any problem due to illumination, occlusions, change of pose, etc. In a more realistic database, the capability of extracting these landmarks with a high precision would drop considerably.

Table 5.6: *EER results using landmarks as features and DTW or ED as classifier for protocols 1:3, 2:3, 3:3, 1:1, 2:1 and 3:1*

LM	EER for protocols: 1:3, 2:3, 3:3, 1:1, 2:1, 3:1					
Experiment	1:3	2:3	3:3	1:1	2:1	3:1
LM 14 NormS DTW	2,31%	2,0%	2,01%	12,60%	9,344%	3,35%
LM 14 NormS ED	2,06%	2,00%	2,00%	7,53%	4,81%	2,40%

5.5. Discussion

In this last section of the chapter, we analyze and evaluate all the methods proposed in the previous sections. All protocols described in section 4.3 are considered. Only the higher resolution of contours is used, except for the LM experiment, which only uses 14 points.

Table 5.7 shows all the results for all the experiments considered and includes an extra column showing the average performance of each type of protocols: protocols *x:3* and protocols *x:1*. From the table, we conclude that the best methods are CC 2800 NormS DTW, SC 2800 NormS DTW and LM 14 NormS ED. With the *x:3* protocols, we obtained higher performance than we we use *x:1* protocols.

However, if we compare the CC 2800 NormS DTW configuration and the SC 2800 NormS DTW configuration we need to evaluate also the computational cost of each case in order to

Table 5.7: *Comparison between CC-DTW, CC-ED, SC-DTW, SC-ED, FD-DTW, FD-ED, LM-DTW methods for protocols 1:3, 2:3, 3:3, 1:1, 2:1 and 3:1*

	EER for protocols: 1:3, 2:3, 3:3, 1:1, 2:1, 3:1							
Experiment	1:3	2:3	3:3	Average	1:1	2:1	3:1	Average.
CC 2800 NormS DTW	1,33%	1,17%	1,51%	1,33%	9,89%	6,78%	1,33%	6,00%
CC 2800 NormS ED	5,33%	5,33%	4,89%	5,18%	9,33%	8,22%	7,67%	8,40%
SC 2800 NormS DTW	2,00%	2,00%	2,00%	2,00%	6,09%	3,33%	2,48%	3,96%
SC 2800 NormS ED	10,00%	8,66%	9,18%	9,28%	16,26%	15,11%	13,25%	14,87%
FD 2800 NormS DTW	4,28%	4,95%	5,55%	4,93%	6,84%	6,88%	7,33%	7,02%
FD 2800 NormS ED	2,43%	3,33%	4%	3,25%	5,61%	5,40%	5,22%	5,41%
LM 14 NormS DTW	2,31%	2,0%	2,01%	2,10%	12,60%	9,344%	3,35%	8,43%
LM 14 NormS ED	2,06%	2,00%	2,00%	2.02%	7,53%	4,81%	2,40%	4,91%

be able to give a reliable decision. In this case, the amount of time investing in computing the EER for the SC 2800 NormS DTW configuration exceed at least ten times the time investing in computing the EER for the CC 2800 NormS DTW configuration. This is because of the difference of dimensionality between these two cases. If in the first case, every subject is modeled with a $2 \times N$ points-vector, the SC configurations needs $60 \times N$ points-vector to model each subject.

On the other hand, if we evaluate the LM 14 NormS ED configuration, we observe that its average EER is better than the average for the CC 2800 NormS DTW. Nevertheless, we need to bear in mind what was said in section 5.4, that these few points are acquired from ideal images, which is not the real case.

Besides, comparing the single EER rate for protocol 3:1, which is one of the most suitable to implement in practical environments, we observe that we have a relative improvement of $46,37\%$ when using the Contour Coordinates instead of the Shape Contexts descriptor, and $44,6\%$ when using the Contour Coordinates instead of the Landmarks.

The worst scenarios are those which use CC with ED and SC with ED. Comparing every pair of experiments changing its classifier between DTW and ED, we confirm that ED is not suitable when using Contour Coordinates or Shape Contexts as features, but it helps to improve the results when we utilize Fourier Descriptors or Landmarks as features.

When analyzing the DET curves depicted in Fig. 5.2 for protocols 3:3 and 3:1 respectively, we obtain the same conclusions. In fact, the best curve for both protocols is CC-2800 NormS DTW curve and the worst is SC-2800 NormS ED curve, as it has been mentioned when comparing the EER results. It is also worth noting that the amount of scores in the curves for protocol 3:3 is lower than the curves drawn for protocol 3:1.

Finally, the results achieved in this work can be compared to previous experiments using the

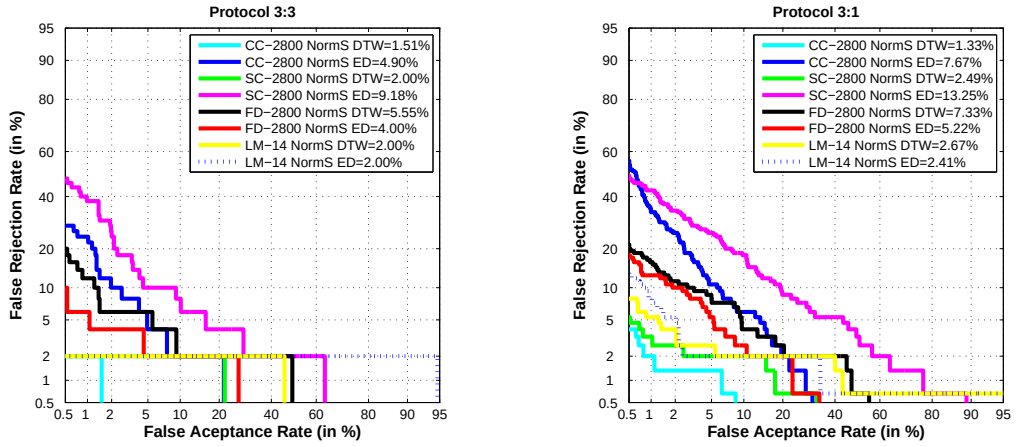

(a) (b)

Figure 5.2: *DET Curve for CC-DTW, CC-ED, SC-DTW, SC-ED, FD-DTW, FD-ED, LM-DTW, LM-ED for protocol 3:3 (a) and for protocol 3:1 (b)*

same database and protocols [Moreno-Moreno *et al.*, 2012]. In that work, the biometric system was based on 21 geometric distances between different key points of the contour. In that case, results of 2% EER were achieved for the protocols 1:3, 2:3 and 3:3. In this work we obtain an average relative improvement of 33.17% EER for the best case (CC 2800 NormS DTW), having in average 1.33% EER.

For protocols 1:1, 2:1, 3:1 we do not achieve to improve the results for protocols 1:1 and 2:1, but at least we achieve the same results than Moreno Moreno [2012], $1,33\%$. This previous work by Moreno-Moreno *et al.* [2012] also applied a SFFS feature selection algorithm improving their EER results very significantly.

Table 5.8 summarizes all experiments carried out in this work. The experiments are classified according to the kind of features used: Contour Coordinates (CC), Shape Contexts (SC), Fourier Descriptors (FD) and Landmarks (LM).

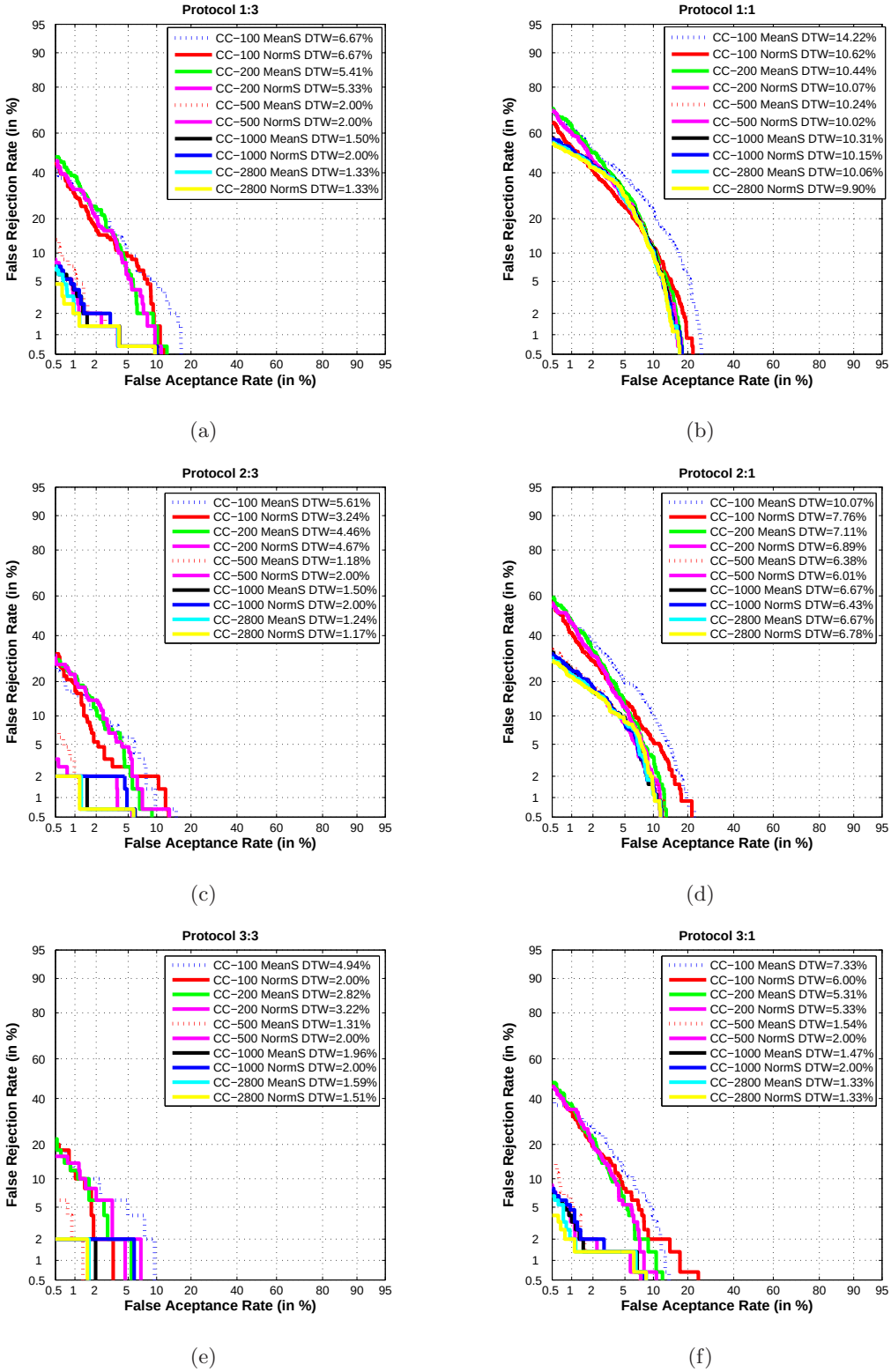

Figure 5.3: *DET Curve for contour coordinates as features and DTW as classifier changing the resolution of the contour and with NormS or MeanS contours for protocols 1:3 (a), 1:1 (b), 2:3 (c), 2:1 (d), 3:3 (e) and 3:1(f)*

Table 5.8: *Experiments carried out in this work for protocols 1:3, 2:3, 3:3, 1:1, 2:1 and 3:1. A color code is also applied. The darker red colors means a low performance of the system while the darker green colors shows a high performance of the system. The best EER results from all experiments are also framed*

		EER for protocols: 1:3, 2:3, 3:3, 1:1, 2:1, 3:1					
Nº	Experiment	1:3	2:3	3:3	1:1	2:1	3:1
1	CC 100 MeanS DTW	6,66%	5,60%	4,93%	14,22%	10,07%	7,33%
2	CC 100 NormS DTW	6,66%	3,23%	2,00%	10,62%	7,75%	6,00%
3	CC 200 MeanS DTW	5,41%	4,46%	2,81%	10,44%	7,11%	5,30%
4	CC 200 NormS DTW	5,33%	4,66%	3,22%	10,07%	6,89%	5,33%
5	CC 500 MeanS DTW	2,00%	1,18%	1,30%	10,23%	6,37%	1,53%
6	CC 500 NormS DTW	2,00%	2,00%	2,00%	10,02%	6,00%	2,00%
7	CC 1000 Means DTW	1,49%	1,49%	1,95%	10,31%	6,66%	1,46%
8	CC 1000 NormS DTW	2,00%	2,00%	2,00%	9,33%	6,42%	2,00%
9	CC 2800 MeanS DTW	1,33%	1,23%	1,59%	10,06%	6,66%	1,33%
10	CC 2800 NormS DTW	1,33%	1,17%	1,51%	9,89%	6,78%	1,33%
11	CC 2800 NormS ED	5,33%	5,33%	4,89%	9,33%	8,22%	7,67%
12	CC 1000 NormS ED	5,33%	5,33%	4,89%	9,33%	8,22%	7,67%
13	CC 500 NormS ED	5,33%	5,33%	4,89%	9,33%	8,22%	7,67%
14	CC 200 NormS ED	5,33%	5,33%	4,85%	9,28%	8,22%	7,55%
15	SC 2800 NormS DTW	2,00%	2,00%	2,00%	6,09%	3,33%	2,48%
16	SC 1000 NormS DTW	2,00%	2,66%	2,00%	9,57%	5,04%	4,00%
17	SC 500 NormS DTW	2,38%	2,00%	2,00%	9,84%	5,77%	4,00%
18	SC 200 NormS DTW	3,91%	2,00%	2,00%	10,66%	6,23%	4,66%
19	SC 2800 NormS ED	10,0%	8,66%	9,18%	16,26%	15,11%	13,25%
20	FD 2800 MeanS DTW	3,30%	3,33%	4,00%	5,33%	5,29%	5,14%
21	FD 2800 NormS DTW	4,28%	4,95%	5,55%	6,8481%	6,88%	7,33%
22	FD 2800 NormS ED	2,43%	3,33%	4,00%	5,61%	5,40%	5,22%
23	LM 14 NormS DTW	2,31%	2,00%	2,01%	12,60%	9,344%	3,35%
24	LM 14 NormS ED	2,06%	2,00%	2,00%	7,53%	4,81%	2,40%

Chapter 6

Conclusions and Future Work

6.1. Conclusions

In this work, a complete body-shape based biometric system has been developed for MMW body images extracted from BIOGIGA database. We have mentioned in Chapter 2 that the use of MMW images instead of images acquired at other spectral bands presents some advantages, mainly the transparency of clothing at that frequency allowing to extract easily the contours from the images.

The main objective of this work consists of building a biometric system using the information of the human contour extracted from images at 94 GHz. The methods proposed in this Dissertation improve the performance of previous works based on geometric measures between key points of the contour carried out over the same database. Even more, we consider that the system based on contour information is much more robust and suitable for real MMW images than the distance-based system, whose capability of extracting body landmarks would drop drastically with real MMW images.

To this aim, we have proposed different features such as using the Contour Coordinates (CC) and three other extracted from the Contour Coordinates such as Shape Contexts descriptor (SC), Fourier Descriptors (FD) and body LandMarks (LM). For classifiers we have studied the Euclidean Distance (ED) as a baseline classifier and the DTW algorithm as an alternative and more complex classifier. Some of these approaches have been studied more in depth in Chapter 3.

In chapter 4, we described the BIOGIGA database and the proccess carried out to extract the body contours from images. In Chapter 5 the experimental framework and protocols followed during the experiments are outlined. In this last chapter, we have studied all the experiments with the objective of finding the best configuration of techniques that yield the best performance of the system. In particular, we have divided the experiments according to the feature used: CC, SC, FD and LM. For each case, we compared the results obtained with the two proposed classifiers. In the majority of the experiments we also study the influence of the resolution of

the contours.

We also accomplished a comparison between the different features used. We conclude that the best results are obtained when using the DTW algorithm directly to the Contour Coordinates for the contours with the highest resolution: 2800 points. In this case we get obtain results of $1,33\%$ for protocols 1:3 and 3:1.

The best case, CC 2800 NormS DTW, has a relative improvement of 33% EER compared to previous works based on geometric measures between key points of the contour carried out over the same database [Moreno-Moreno *et al.*, 2011b, 2012].

Considering all protocols evaluated (1:3, 2:3, 3:3, 1:1, 2:1, 3:1), we conclude that the best protocols to use in a body-shape based biometric system are those which can have a more robust model of the subject, that is: protocols 3:3 and 3:1 as they include 3 images per person in the train stage. Besides, having a protocol 3:3 is not very common in realistic scenarios. For this reason, protocol 3:1 is the most suitable protocol to consider when building a commercial body-shape based biometric system.

The limitations of this work are related to the special characteristics of the database used. Images from BIOGIGA database are limited when compared to real images acquired in practice, but there are not publicly available databases for the moment. In our case, the synthetic images were obtained from measures of real people and are similar to some extent to real data captured at 94 GHz [Alefs *et al.*, 2010]

6.2. Future Work

For future work, we propose to keep investigating other techniques or a combination of techniques that may improve even more the performance of the system. We also have in mind to carry out a fusion of the body-shape based biometric system proposed in this work, and the geometric-based biometric system proposed by [Moreno-Moreno *et al.*, 2011b]. Another major area of interest is to apply all the techniques proposed in this Dissertation to a real database. This would allow to have a more reliable vision of the approaches described and evaluated in this work.

In real data, other information such as the texture of the human body can be also extracted and could be used for person recognition.

Chapter 7

Glossary

- **AI**: Active Indoors (referring to imaging system).
  Active imaging system working indoors. See AMMW or ASMW.
- **AMMW**: Active Millimeter Wave (Imaging System).
  Imaging system that emits millimeter wave radiation to the scene and then collects the reflected radiation to form the image.
- **AO**: Active Outdoors (referring to imaging system).
  Active imaging system working outdoors. See AMMW or ASMW.
- **ASMW**: Active Subillimeter Wave (Imaging System).
  Imaging system that emits submillimeter wave radiation to the scene and then collects the reflected radiation to form the image.
- ***CC***: Contour Coordinates.
  In some cases, we use the contour coordinates as features of the system.
- ***cr***: With Clothing (from the Spanish expression "con ropa").
  Abbreviation used to describe the clothing condition of a user in the images used in the experiments.
- **DET**: Detection Error Tradeoff Curve.
  Curve widely used to show graphically the verification performance of a biometric system. It plots the FRR versus the FAR for all the different threshold values with logarithmic axes.
- **DTW**: Dyamic Time Warping.
  A dynamic programming technique whose aim is to find an elastic match among of a pair of sequences that minimizea given distance measure.
- **ED**: Euclidean Distance.
  It the naive metric distance between two sequences of points in any dimension.

- **EER**: Equal Error Rate.
  Error rate at which both error rates (FRR and FAR) coincide, for a certain threshold value.

- **FAR**: False Acceptance Rate.
  Probability that an impostor is accepted by a biometric system as a genuine user.

- **FD**: Fourier Descriptors.
  Descriptors which convert the coordinates of a shape into complex numbers, and then applies the Fourier transform.

- **FRR**: False Rejection Rate.
  Probability that a genuine user is rejected by a biometric system.

- **IR**: Infrared.
  Electromagnetic radiation with wavelength in the range of 0.7-100 μm ($4.3{\cdot}10^{14}$-$3{\cdot}10^{12}$ Hz).

- **LM**: LandMark.
  A small set of points that describe the most discriminative points of a shape.

- **LWIR**: Long Wave Infrared.
  Infrared radiation with wavelength in the range of 8-14 μm.

- **MeanS**: Mean Size.
  With this configuration, the contours belonging to the same user do not have the same dimensionality altough the variation is restricted to 20-30 points.

- **MMW**: Millimeter Waves.
  Electromagnetic radiation that, together with the submillimeter waves, fills the gap between the infrared and microwave bands in the electromagnetic spectrum. Millimeter waves lie in the band of 1-10 mm (300-30 GHz). Clothing is highly transparent to the MMW radiation.

- **MWIR**: Medium Wave Infrared.
  Infrared radiation with wavelength in the range of 3-5 μm.

- **NIR**: Near Infrared.
  Infrared radiation with wavelength in the range of 0.7-1 μm.

- **NormS**: Normalized Size.
  With this configuration, all the contours belonging to the same user have the same dimensionality.

- **PI**: Passive Indoors (referring to imaging system).
  Passive imaging system working indoors. See PMMW or PSMW.

- **PMMW**: Passive Millimeter Wave (Imaging System).
  Imaging system that collects natural millimeter wave radiation that has been emitted and reflected from the scene, to form the image.
- **PO**: Passive Outdoors (referring to imaging system).
  Passive imaging system working outdoors. See PMMW or PSMW.
- **PSMW**: Passive Submillimeter Wave (Imaging System).
  Imaging system that collects natural submillimeter wave radiation that has been emitted and reflected from the scene, to form the image.
- **SC**: Shape Contexts descriptor.
  A complex descriptor that describes each point within a shape by pointing out the relative distance and angle of the remainder points of the shape through a log-polar histogram.
- **SMW**: Submillimeter Waves.
  Electromagnetic radiation that, together with the millimeter wave radiation, fills the gap between the infrared and microwave bands in the electromagnetic spectrum. Submillimeter waves lie in the range of 0.1-1 mm (0.3-3 THz). Clothing is partially transparent to the SMW radiation.
- ***sr***: Without Clothing (from the Spanish expression "sin ropa").
  Abbreviation used to describe the clothing condition of a user in the images used in the experiments.
- **SWIR**: Short Wave Infrared.
  Infrared radiation with wavelength in the range of 1-3 μm.
- **VIS**: Visible Spectrum.
  Portion of the electromagnetic spectrum that is visible to the human eye. Electromagnetic radiation in this range of wavelengths (400-700 nm) is usually called light.
- **VLWIR**: Very Long Wave Infrared.
  Infrared radiation with wavelength in the range of 14-100 μm.
- **XR**: X-ray.
  Electromagnetic radiation with a wavelength that lies between 0.01-10 nm ($3{\cdot}10^{19}$-$3{\cdot}10^{16}$ Hz).

Appendix A

Publications

Part of the work of this Dissertation has been accepted in the ICCST Conference that will take place in Medellín, Colombia on 8-11th October.

- **E. González-Sosa**, R. Vera-Rodríguez, J. Fiérrez and Javier Ortega, "Body Shape-based Biometric Recognition using Millimeter Wave Images", in Proc. IEEE Int. Carnahan Conf. on Security Technology, ICCST, 2013.

Appendix B

Short Biography

Ester Gonzalez Sosa was born in 1988 in Las Palmas de Gran Canaria. She started her Electrical Engineering in 2006 and received the MSc degree in 2012 from Universidad de Las Palmas de Gran Canaria, Spain. Since September of 2012, she is with the Biometric Recognition Group - ATVS at the Universidad Autonoma de Madrid, where she is currently collaborating as an assistant researcher pursuing the PhD degree. Her research interests include signal and image processing, pattern recognition, computer vision and biometrics. Her current research focuses on soft biometrics and biometric recognition in the MMW band.

References

http://www.iaa.gov.il/Rashat/en-US/Airports/BenGurion/InformationforTravelers/Services/BiometricPassportControlCheck/ 5

http://uidai.gov.in/about-uidai.html. 5

B. Alefs, R. den Hollander, F. Nennie, E. van der Houwen, M. Bruijn, W. van der Mark, and J. Noordam. Thorax biometrics from millimetre-wave images. *Pattern Recognition Letters*, 31(15):2357–2363, 2010. 1, 6, 10, 14, 27, 30, 48

R. Appleby and R. N. Anderton. Millimeter-wave and submillimeter-wave imaging for security and surveillance. *Proceedings of the IEEE*, 95(8):1683–1690, 2007. 6, 15

S. Belongie, J. Malik, and J. Puzicha. Shape matching and object recognition using shape contexts. *Pattern Analysis and Machine Intelligence, IEEE Transactions on*, 24(4):509–522, 2002. 19, 20, 39

J. E. Bjarnason, T. L. J. Chan, A. W. M. Lee, M. A. Celis, and E. R. Brown. Millimeter-wave, terahertz, and mid-infrared transmission through common clothing. *Applied Physics Letters*, 85(4):519–521, 2004. URL `http://link.aip.org/link/?APL/85/519/1`. 15

Blender. http://blender.org/, 2011. 27

P. Buddharaju, I. T. Pavlidis, P. Tsiamyrtzis, and M. Bazakos. Physiology-based face recognition in the thermal infrared spectrum. *Pattern Analysis and Machine Intelligence, IEEE Transactions on*, 29(4):613–626, 2007. xi, 11, 12

H. Chen and A. K. Jain. Dental biometrics: Alignment and matching of dental radiographs. In *Application of Computer Vision, 2005. WACV/MOTIONS'05 Volume 1. Seventh IEEE Workshops on*, volume 1, pages 316–321. IEEE, 2005. 1, 6, 12

X. Chen, P. J. Flynn, and K. W. Bowyer. Ir and visible light face recognition. *Computer Vision and Image Understanding*, 99(3):332–358, 2005. xi, 12

K. Cooper, R. Dengler, N. Llombart, T. Bryllert, G. Chattopadhyay, E. Schlecht, J. Gill, C. Lee, A. Skalare, I. Mehdi, and P. Siegel. Penetrating 3-d imaging at 4- and 25-m range using a submillimeter-wave radar. *Microwave Theory and Techniques, IEEE Transactions on*, 56(12):2771 –2778, dec. 2008. ISSN 0018-9480. xi, 15, 16

T. Derham, H. Kamoda, T. Iwasaki, and T. Kuki. Active mmw imaging system using the frequency-encoding technique. In *Microwave Conference, 2007. KJMW 2007. Korea-Japan*, pages 181 –184, nov. 2007. 14

M. Ferrer, A. Morales, and L. Ortega. Infrared hand dorsum images for identification. *Electronics letters*, 45(6): 306–308, 2009. 11

P. Gloor. Bertillon's method and anthropological research; a new use for old anthropometric files. *Journal of the Forensic Science Society*, 20(2):99–101, 1980. 2

R. Howald, G. Clark, J. Hubert, and D. Ammar. Millimeter waves: The evolving scene. In *Technologies for Homeland Security, 2007 IEEE Conference on*, pages 234 –239, may 2007. 13

A. K. Jain, R. M. Bolle, and S. Pankanti. *Biometrics: personal identification in networked society*. Springer, 1999. 1, 2, 32

A. K. Jain, F. D. Griess, and S. D. Connell. On-line signature verification. *Pattern recognition*, 35(12):2963–2972, 2002. 6, 24

A. K. Jain, A. Ross, and S. Prabhakar. An introduction to biometric recognition. *Circuits and Systems for Video Technology, IEEE Transactions on*, 14(1):4–20, 2004. 2, 4

A. K. Jain, A. A. A. Ross, and K. Nandakumar. *Introduction to biometrics*. Springer, 2011. 1

B. Kapilevich, B. Litvak, M. Einat, and O. Shotman. Passive mm-wave sensor for in-door and out-door homeland security applications. In *Sensor Technologies and Applications, 2007. SensorComm 2007. International Conference on*, pages 20 –23, oct. 2007. 13

A. Kholmatov and B. Yanikoglu. Identity authentication using improved online signature verification method. *Pattern recognition letters*, 26(15):2400–2408, 2005. 24, 25

A. Lee, B. Williams, S. Kumar, Q. Hu, and J. Reno. Real-time imaging using a 4.3-thz quantum cascade laser and a 320 /spl times/ 240 microbolometer focal-plane array. *Photonics Technology Letters, IEEE*, 18(13):1415 –1417, july 2006. ISSN 1041-1135. 16

S. Z. Li, R. Chu, S. Liao, and L. Zhang. Illumination invariant face recognition using near-infrared images. *Pattern Analysis and Machine Intelligence, IEEE Transactions on*, 29(4):627–639, 2007. XI, 1, 6, 11, 12

C.-L. Lin and K.-C. Fan. Biometric verification using thermal images of palm-dorsa vein patterns. *Circuits and Systems for Video Technology, IEEE Transactions on*, 14(2):199–213, 2004. 12

A. Luukanen, L. Grönberg, T. Haarnoja, P. Helistö, K. Kataja, M. Leivo, A. Rautiainen, J. Penttilä, J. Bjarnason, C. Dietlein, *et al.* Passive thz imaging system for stand-off identification of concealed objects: results from a turn-key 16 pixel imager. In *SPIE Defense and Security Symposium*, pages 69480O–69480O. International Society for Optics and Photonics, 2008. XI, 16

A. Luukanen, E. Grossman, A. Miller, P. Helisto, J. Penttila, H. Sipola, and H. Seppa. An ultra-low noise superconducting antenna-coupled microbolometer with a room-temperature read-out. *Microwave and Wireless Components Letters, IEEE*, 16(8):464 –466, aug. 2006. ISSN 1531-1309. 15

J. Mait, D. Wikner, M. Mirotznik, J. van der Gracht, G. Behrmann, B. Good, and S. Mathews. 94-GHz imager with extended depth of field. *Antennas and Propagation, IEEE Transactions on*, 57(6):1713 –1719, june 2009. ISSN 0018-926X. 6, 13

MakeHuman. http://makehuman.org/, 2011. 27

R. Martens and L. Claesen. Dynamic programming optimisation for on-line signature verification. In *Document Analysis and Recognition, 1997., Proceedings of the Fourth International Conference on*, volume 2, pages 653–656. IEEE, 1997. 25

M. Martínez-Díaz. Dyanmic signature verification for portable devices. Master's thesis, Universidad Autónoma de Madrid, November 2008. XII, 24, 25

K. Mikolajczyk and C. Schmid. A performance evaluation of local descriptors. *Pattern Analysis and Machine Intelligence, IEEE Transactions on*, 27(10):1615–1630, 2005. 18

M. Moreno Moreno. Reconocimiento biométrico basado en imágenes simuladas en la banda de ondas milimétricas. Master's thesis, Universidad Autónoma de Madrid, June 2012. 9, 22, 28, 29, 42, 44

M. Moreno-Moreno, J. Fierrez, and J. Ortega-Garcia. Biometrics beyond the visible spectrum: Imaging technologies and applications. In *Proc. Biometric ID Management and Multimodal Communication*, pages 154–161. Springer, 2009. 6

M. Moreno-Moreno, J. Fierrez, P. Tome, R. Vera-Rodriguez, J. Parron, and J. Ortega-Garcia. Biogiga: Base de datos de imagenes sinteticas de personas a 94 ghz con fines biometricos. 2011a. XII, 6, 27, 28

M. Moreno-Moreno, J. Fierrez, R. Vera-Rodriguez, and J. Parron. Distance-based feature extraction for biometric recognition of millimeterwave body images. In *Proc. IEEE Intl. Carnahan Conf. on Security Technology, ICCST*, pages 326–331, 2011b. 1, 6, 7, 10, 14, 48

M. Moreno-Moreno, J. Fierrez, R. Vera-Rodriguez, and J. Parron. Simulation of millimeter wave body images and its application to biometric recognition. In *Proc. International Conferencie SPIE Defense Security and Sensing, SPIE*, volume 8362, pages 83620E–1, 2012. 30, 32, 44, 48

E. Persoon and K.-S. Fu. Shape discrimination using fourier descriptors. *IEEE Transactions on Systems, Man and Cybernetics*, 7(3):170–179, 1977. ISSN 0018-9472. 19

D. T. Petkie, C. Casto, F. C. D. Lucia, S. R. Murrill, B. Redman, R. L. Espinola, C. C. Franck, E. L. Jacobs, S. T. Griffin, C. E. Halford, J. Reynolds, S. O'Brien, and D. Tofsted. Active and passive imaging in the thz spectral region: phenomenology, dynamic range, modes, and illumination. *J. Opt. Soc. Am. B*, 25(9):1523–1531, 2008. URL `http://josab.osa.org/abstract.cfm?URI=josab-25-9-1523`. 15

S. Prabhakar, S. Pankanti, and A. K. Jain. Biometric recognition: Security and privacy concerns. *Security & Privacy, IEEE*, 1(2):33–42, 2003. 5

A. Richards. *Alien vision: exploring the electromagnetic spectrum with imaging technology*, volume 104. SPIE Press, 2001. 9

A. A. Ross, K. Nandakumar, and A. K. Jain. *Handbook of multibiometrics*, volume 6. Springer, 2006. 4

M. Sato, T. Hirose, T. Ohki, H. Sato, K. Sawaya, and K. Mizuno. 94-GHz band high-gain and low-noise amplifier using inp-hemts for passive millimeter wave imager. In *Microwave Symposium, 2007. IEEE/MTT-S International*, pages 1775 –1778, june 2007. 13, 25

A. Selinger and D. A. Socolinsky. Face recognition in the dark. *Computer Vision and Pattern Recognition Workshop*, 8:129, 2004. ISSN 1063-6919. 12

L. Shamir, S. Ling, S. Rahimi, and L. Ferrucci. Biometric identification using knee x-rays. *International journal of biometrics*, 1(3):365–370, 2009. 1

D. Sheen, D. McMakin, and T. Hall. Three-dimensional millimeter-wave imaging for concealed weapon detection. *Microwave Theory and Techniques, IEEE Transactions on*, 49(9):1581 –1592, sep 2001. ISSN 0018-9480. XI, 14

D. Sheen, D. McMakin, T. Hall, and R. Severtsen. Active millimeter-wave standoff and portal imaging techniques for personnel screening. In *Technologies for Homeland Security, 2009. HST '09. IEEE Conference on*, pages 440 –447, 11-12 2009. 14, 16

X. Shen, C. Dietlein, E. Grossman, Z. Popovic, and F. Meyer. Detection and segmentation of concealed objects in terahertz images. *Image Processing, IEEE Transactions on*, 17(12):2465 –2475, dec. 2008. ISSN 1057-7149. xi, 15, 16

G. Sinclair, P. Coward, R. Anderton, R. Appleby, T. Seys, and P. Southwood. Detection of illegal passengers in lorries using a passive millimetre wave scanner. In *Security Technology, 2002. Proceedings. 36th Annual 2002 International Carnahan Conference on*, pages 167 – 170, 2002. 13

A. Tamminen, J. Ala-Laurinaho, and A. Raisanen. Indirect holographic imaging at 310 ghz. In *Radar Conference, 2008. EuRAD 2008. European*, pages 168 –171, oct. 2008. 16

S. Theodoridis, A. Pikrakis, K. Koutroumbas, and D. Cavouras. *Introduction to Pattern Recognition: A Matlab Approach: A Matlab Approach*. Access Online via Elsevier, 2010. 21

Thruvision. http://www.digitalbarriers.com/products/thruvision/. 15

G. Timms, J. Bunton, M. Brothers, and J. Archer. 190 GHz millimetre-wave imaging using mmic-based heterodyne receivers. In *Wireless Broadband and Ultra Wideband Communications, 2007. AusWireless 2007. The 2nd International Conference on*, page 32, aug. 2007. 14

L. Wang and G. Leedham. Near- and far- infrared imaging for vein pattern biometrics. *Advanced Video and Signal Based Surveillance, IEEE Conference on*, 0:52, 2006. 12

www.alfaimaging.com. http://www.alfaimaging.com/. xi, 14

www.vision4thefuture.org. http://vision4thefuture.org/. xi, 14

M. Yang, K. Kpalma, J. Ronsin, *et al.* A survey of shape feature extraction techniques. *Pattern recognition*, pages 43–90, 2008. xi, 17, 18, 20

M. Yasuhara and M. Oka. Signature verification experiment based on nonlinear time alignment: a feasibility study. *IEEE Trans. Systems Man Cybernet*, 17:212–216, 1977. 20, 23

E. Yoruk, E. Konukoglu, B. Sankur, and J. Darbon. Shape-based hand recognition. *IEEE Transactions on Image Processing*, 15(7):1803–1815, 2006. ISSN 1057-7149. 6

L. Yujiri, M. Shoucri, and P. Moffa. Passive millimeter wave imaging. *Microwave Magazine, IEEE*, 4(3):39–50, 2003. 6, 13

D. Zhang and G. Lu. Review of shape representation and description techniques. *Pattern recognition*, 37(1):1–19, 2004. 17

H. Zhang and J. Malik. Learning a discriminative classifier using shape context distances. In *Computer Vision and Pattern Recognition, 2003. Proceedings. 2003 IEEE Computer Society Conference on*, volume 1, pages I–242. IEEE, 2003. xi, 21